⌘ *Author's Choice*

# Extracellular and Luminal pH Regulation by Vacuolar H$^+$-ATPase Isoform Expression and Targeting to the Plasma Membrane and Endosomes*

**Gina A. Smith**[‡1], **Gareth J. Howell**[‡2], **Clair Phillips**[§], **Stephen P. Muench**[§3], **Sreenivasan Ponnambalam**[‡4], **and Michael A. Harrison**[§5]

*From the ‡Endothelial Cell Biology Unit, School of Molecular and Cellular Biology and §School of Biomedical Sciences, Faculty of Biological Sciences, University of Leeds, Leeds LS2 9JT, United Kingdom*

**Plasma membrane vacuolar H$^+$-ATPase (V-ATPase) activity of tumor cells is a major factor in control of cytoplasmic and extracellular pH and metastatic potential, but the isoforms involved and the factors governing plasma membrane recruitment remain uncertain. Here, we examined expression, distribution, and activity of V-ATPase isoforms in invasive prostate adenocarcinoma (PC-3) cells. Isoforms 1 and 3 were the most highly expressed forms of membrane subunit $a$, with $a_1$ and $a_3$ the dominant plasma membrane isoforms. Correlation between plasma membrane V-ATPase activity and invasiveness was limited, but RNAi knockdown of either $a$ isoform did slow cell proliferation and inhibit invasion *in vitro*. Isoform $a_1$ was recruited to the cell surface from the early endosome-recycling complex pathway, its knockdown arresting transferrin receptor recycling. Isoform $a_3$ was associated with the late endosomal/lysosomal compartment. Both $a$ isoforms associated with accessory protein Ac45, knockdown of which stalled transit of $a_1$ and transferrin-transferrin receptor, decreased proton efflux, and reduced cell growth and invasiveness; this latter effect was at least partly due to decreased delivery of the membrane-bound matrix metalloproteinase MMP-14 to the plasma membrane. These data indicate that in prostatic carcinoma cells, $a_1$ and $a_3$ isoform populations predominate in different compartments where they maintain different luminal pH. Ac45 plays a central role in navigating the V-ATPase to the plasma membrane, and hence it is an important factor in expression of the invasive phenotype.**

The vacuolar H$^+$-ATPase has emerged as a significant contributor to net proton efflux from tumor cells (1–4). This 1-MDa membrane complex, comprising the soluble catalytic V$_1$ domain coupled to an integral membrane domain V$_o$, uses the free energy of cytosolic ATP hydrolysis to pump protons across membrane bilayers (5, 6). Also a ubiquitous component of endomembranes, the V-ATPase acidifies compartments involved in all stages of vesicular transport (6). Plasma membrane V-ATPases are not unique to tumor cells and also play crucial roles in acid efflux from osteoclasts, epididymal clear cells, and renal intercalated cells (7, 8).

The ATP-hydrolyzing V$_1$ domain contains subunits A–H in a stoichiometry (AB)$_3$CDE$_3$FG$_3$H. V$_o$ translocates protons across the membrane and consists of $a$, $d$, and $e$ subunits linked to a 6–10-member ring of $c$ subunits. Operating as a rotary motor, proton translocation is postulated to take place at the dynamic interface of the $a$ subunit and $c$-ring in the membrane (see Ref. 5 and references therein). In higher eukaryotes, most subunits occur as multiple isoforms (9, 10). For many, a common ubiquitous form predominates with others expressed at high levels in particular tissues. The B$_1$ subunit (ATP6V1B1), for example, is highly expressed in kidney, with naturally occurring mutations causing distal renal tubular acidosis, whereas B$_2$ is ubiquitously expressed (11). Vertebrates express subunit $a$ isoforms 1–4 (plus additional splice variants) that have 47–61% sequence identity (12, 13). Although individual subunit $a$ isoforms are particularly highly expressed in some cells, multiple forms are generally present and targeted to specific compartments (14, 15). Targeting may be a function of the cytoplasmic N-terminal domain of the protein, as it is in the budding yeast *Saccharomyces cerevisiae* (16). The $a_1$ form (ATP6V0A1) appears ubiquitous, with some variants particularly abundant in neuronal tissue (17), whereas $a_3$ (ATP6V0A3) is highly expressed in osteoclasts and macrophages (14, 18). The predominant species in cells of the kidney and male reproductive tract is $a_4$ (19, 20). The $a_2$ form has been detected in early endosomes (21) and in the Golgi complex (14, 22, 23), with mutations causing the glycosylation defects and aberrant trafficking that are characteristic of the disease cutis laxa (22). The $a_3$ form is found in late endosomes/lysosomes of cells of monocytic lineage from where it is recruited to the ruffled border zone of the plasma membrane of active osteoclasts or to the maturing phagosome of macrophages (14, 18). In pancreatic β-cells, $a_3$ is targeted to insulin-secreting granules (24), although the $a_1$ form has been identified in secretory vesicles in neuroendocrine PC12 cells (23). The $a_1$ isoform is also found in synaptic vesicles of neuronal cells (17), performing the follow-

ing two distinct roles: proton pumping to energize neurotransmitter loading into vesicles, and $Ca^{2+}$-regulated vesicle fusion with the plasma membrane involving $V_o$ interaction with the R-SNARE synaptobrevin (VAMP2) (25, 26). Consequently, $V_o$ containing subunit $a_1$ is likely to appear at least transiently at the plasma membrane of neuronal cells (17), although not necessarily actively coupled to $V_1$. The $a_1$, $a_3$, and $a_4$ forms are also featured at the plasma membrane of kidney proximal tubule cells, in which $a_2$ appears to be localized to early endosomes (21). In renal intercalated cells and epididymal clear cells, $a_4$ is targeted to the apical membrane (27). Currently, little is known about either the functional differences between subunit isoforms or the rules governing the interactions they make, but it is feasible that eukaryotic cells could assemble a wide variety of V-ATPase complexes with potentially different functional properties, locations, and inhibitor sensitivity.

Plasma membrane V-ATPase activity is linked to growth and invasiveness of a number of neoplastic cell types, including breast (1, 3, 28, 29) and prostate (30, 31). Expression of the subunit $a_3$ isoform is higher in invasive melanoma cells compared with non-invasive controls (32), and the same subunit is also implicated in invasiveness of breast cancer cells (33). The $a_4$ subunit is highly expressed in some gliomas (34). V-ATPase activity is proposed to contribute to tumor cell invasiveness and growth via the following three mechanisms: first, maintaining the acidic extracellular pH ($pH_{ex}$) promotes activity of cathepsins and activation of matrix metalloproteases (30, 32, 35, 36) that can remodel the ECM[6] to facilitate tumor cell extravasation and invasion of adjacent tissues; second, by contributing to the stability of the abnormally alkaline cytosolic pH ($pH_{cyt}$) of tumor cells (37), the V-ATPase helps the cell evade acidosis-induced apoptosis (38, 39); and third, V-ATPase activity facilitates sequestration of some chemotherapeutic drugs in intracellular compartments leading to drug resistance (29, 40, 41). The sensitivity of tumor cells to loss of V-ATPase function has fueled interest in the enzyme as a therapeutic target in cancer (42, 43), but the ubiquitous nature of the enzyme makes specific targeting of cancer cells problematic. $V_o$ subunit $c$ binds bafilomycin and other lipid-soluble inhibitors (44, 45), but a role for subunit $a$ in inhibitor binding is also likely (46, 47), opening the possibility of discriminatory isoform-specific inhibitors. To support such development, more information is required about the differential expression, relative levels of activities, and functional roles of the different isoforms in cancer cells.

In this study, we have examined the expression of subunit $a$ isoforms in prostatic carcinoma cells and examined their relative contributions to proton efflux activity across the plasma membrane. Using RNAi, we looked at the function of different isoforms in endocytotic processes such as plasma membrane receptor recycling. The accessory subunit Ac45 has been proposed to be a primary factor in V-ATPase relocation to the plasma membrane (48, 49) and in $Ca^{2+}$-regulated exocytosis (50). Here, we investigated the association of this polypeptide with different subunit $a$ iso-

forms and the consequences of its depletion on V-ATPase localization and function in prostate carcinoma cells.

## Experimental Procedures

*Cell Culture*—PC-3 (derived from a grade IV prostatic adenocarcinoma bone metastasis) and LNCaP (lymph node metastasis of prostatic carcinoma) epithelium-like cell lines obtained from ECACC were cultured in Ham's F-12 and RPMI 1640 media, respectively, supplemented with 7% fetal bovine serum and 2 mM glutamine. Cultures were incubated at 37 °C under 5% $CO_2$. For transfer to microphysiometry and invasion assay supports, the adherent cells were released by treatment with Accutase (PAA Laboratories). Two cultures of PC-3 cells used at different stages in this study were both validated by STR profiling (Public Health England Cell Line Authentication Service, Porton Down, UK).

*RNAi Treatment*—Cells cultured in 6-well plates were treated with 19-mer siRNAs targeted against Ac45 (Thermo Scientific-Dharmacon SMARTpool M-021378-00, 25 nM), ATP6V0A1 (Thermo Scientific-Dharmacon SMARTpool M-017618-00, 100 nM), ATP6V0A3 (Thermo Scientific-Dharmacon SMARTpool M-012198-00, 100 nM), and ATP6V1A1 (Thermo Scientific Dharmacon SMARTpool L-017590-01, 50 nM). A control siRNA (Thermo Scientific-Dharmacon non-targeting pool D-001810-10) was also used at 100 nM. The four constituent siRNAs within each pool were also tested individually for effects on expression and for phenotypic effects. As an additional negative control, a representative siRNA from each pool was tested after custom synthesis (Thermo Scientific-Dharmacon) to include nucleotide changes as underlined: $a_1$, caacaucucaguaaugcua; $a_3$, cccucgcgcagcacaagua; Ac45, ccaccugucaacguaguuu).

The siRNAs were incubated with DharmaFECT-2 transfection reagent (Thermo Scientific) in serum-free medium for 45 min at room temperature before mixing 1:4 with complete medium (7% fetal bovine serum). Cells were treated with the siRNA mixture for 24 h before replacement with fresh complete medium. Where necessary for certain assays (invasion, microphysiometry), cells were transferred after this time and used within the subsequent 24 h.

*Microphysiometry*—Measurements of extracellular acidification rate (ECAR) were performed using a Cytosensor microphysiometer (Molecular Devices). Adherent PC-3 cells ($10^5$ cells per cup) were seeded directly into the microphysiometer capsule cups and cultured for 48 h as above to allow an adherent monolayer to form. Weakly adherent LNCaP cells required embedding in agarose to prevent detachment from the capsule membrane. Cups were placed in the sensor chamber containing perfusion buffer (nominally bicarbonate-free Hanks' basal salt solution (HBSS) without HEPES, pH 7.4). For sodium-free HBSS, NaCl was replaced with 138 mM choline to maintain osmolarity. The flow chamber formed between cell monolayer and insert (effective volume 2.6 $\mu$l) was circulated with perfusion buffer at 37 °C at a rate of 100 $\mu$l min$^{-1}$. A pump cycle of 40 s off and 80 s on was used. Typically, cells reached a steady state ECAR after 30–40 min. Rates of acid accumulation are computed by the Cytosensor software as the least squares fit to the raw voltage time trace recorded when the pump is off, and

---

[6] The abbreviations used are: ECM, extracellular matrix; ECAR, extracellular acidification rate; ERC, endosomal recycling complex; HBSS, Hanks' basal salt solution; TfR, transferrin receptor; V-ATPase, vacuolar H$^+$-ATPase; Tf, transferrin.

the derived data are expressed as the change in ECAR as a function of time. Buffering capacity of the perfusion buffer, equilibrated with atmospheric $CO_2$ at 37 °C, was determined by titrating change in pH with increasing concentrations of HCl. Titration curves were linear across the pH range spanned by the experiments. Rates of proton efflux ($J_H^+$, in nM $H^+$ $min^{-1}$) were calculated by first converting ECAR into a rate of change of pH (using the Nernst equation) and then calculating the increase in $H^+$ concentration assuming a starting concentration of 40 nM, pH 7.4. Because the buffering capacity of the perfusion medium was negligible, $J_H^+$ was not corrected for any buffering effects. At 37 °C, a change in $pH_{ex}$ of 1 pH unit $min^{-1}$ is equivalent to a rate of change in potential of 61 mV $s^{-1}$.

Inhibitors were perfused into the assay chamber via electronically switchable valves. Bafilomycin $A_1$, concanamycin A, and ethylisopropylamiloride (Sigma) were introduced from freshly made stock solutions in DMSO. This vehicle had no measurable effects on ECAR.

*Cell Proliferation Assay*—Cells were plated at a density of $1 \times 10^4$ cells/well in a 96-well plate (CellCarrier-96, PerkinElmer Life Sciences) and allowed to adhere for 4 h. Cells were then transfected with siRNAs as above. After culture for 48 h, live cell numbers (relative to control) were determined by uptake of calcein acetoxymethyl ester (calcein-AM; 2.5 $\mu$M, 60 min incubation at 37 °C in HBSS buffer). Fluorescence was measured in a FlexStation 3 (Molecular Devices) with excitation at 490 nm and emission at 520 nm. Numbers of dead cells (as a percentage relative to controls) were determined fluorometrically by propidium iodide uptake (excitation at 535 nm and emission at 617 nm).

*Invasion Assays*—Cell migration through basement membrane extract was assayed using Cultrex basement membrane extract cell invasion assay in a 24- or 96-well plate format (Trevigen Inc., Gaithersburg, MD). Cells were starved overnight in serum-free medium, detached by treatment with Accutase, and resuspended in serum-free medium to give $10^6$ live cells $ml^{-1}$. In the final assay setup, each upper well of the modified Boyden chamber contained $5 \times 10^4$ cells (24-well format) or $0.5 \times 10^4$ cells (96-well format). To test the effects of concanamycin, the inhibitor was added to an aliquot of the cell suspension to give a final concentration of 1 $\mu$M in the upper chamber (0.5% v/v DMSO, also included in control wells). Soluble recombinant receptor activator of nuclear factor $\kappa$B ligand (PeproTech, London, UK) was used at 10 $\mu$g $ml^{-1}$. As chemoattractant, the bottom well of each chamber contained medium supplemented with 10% FBS. Plates were incubated at 37 °C (5% v/v $CO_2$) for 24 h, after which time any cells that had passed through the basement membrane extract/polycarbonate membrane were detached. Cells were quantified by incubating with calcein-AM and measuring the internalized fluorescence signal in a plate reader accessory attached to a Cary Eclipse scanning fluorimeter or FlexStation 3 (excitation at 485 nm and emission at 520 nm).

*Immunoprecipitation and Immunoblotting*—Antibodies used in this study were as follows: mouse anti-subunit A (H-00000523-M02; Abnova Inc., Taiwan) recognizing residues 508–618 of human ATP6V1A; rabbit anti-$a_1$ (sc-28801, Santa Cruz Biotechnology Inc., Dallas, TX) recognizing residues 71–210 of human

ATP6V0A1; rabbit anti-$a_1$ (AP5109A, Generon, UK) recognizing residues 44–71 of human ATP6V0A1; mouse anti-$a_2$ (H00023545-A01, Abnova Inc.) recognizing residues 198–304 of human ATP6V0A2; rabbit anti-$a_3$ made in-house against a peptide comprising residues 689–707 of human ATP6V0A3; rabbit anti-$a_4$ (ab55827, Abcam, UK) recognizing the C-terminal residues of human ATP6V0A4; mouse anti-Ac45 (H00000537-M01, Abnova Inc.) recognizing residues 51–151 of human ATP6AP1; goat anti-ATP6V1F (sc-21220, Santa Cruz Biotechnology, Inc.) recognizing a C-terminal peptide of $V_1$ subunit F; rabbit anti-MMP-14 (AB8102, Millipore (UK) Ltd., Watford, UK), recognizing catalytic domain residues 91–246; mouse anti-CD71 (transferrin receptor; sc-65887, Santa Cruz Biotechnology, Inc.); mouse anti-LAMP-1 (MA1–164, Thermo Fisher); sheep anti-TGN46 (51); and mouse anti-tubulin (T6199 (clone DM1A), Sigma). Whole cell lysates were prepared by solubilization in RIPA buffer (20 mM Tris-HCl, 150 mM NaCl, 1 mM Na-EDTA, 1 mM EGTA, 1% w/v Nonidet P-40, 0.5% sodium deoxycholate, protease inhibitor mixture), centrifugation at 13,000 rpm in a microcentrifuge at 4 °C followed by heating to 80 °C for 10 min. The protein concentration was determined using the BCA method, and the concentration was adjusted to 1 mg $ml^{-1}$ with RIPA buffer. For immunoprecipitation, cells cultured in 6-well plates were washed twice with PBS containing $Mg^{2+}$ and $Ca^{2+}$ (PBS-Mg/Ca) before extraction into RIPA buffer by incubation on ice for 20 min. Cell lysates were centrifuged at $100,000 \times g$ for 20 min at 4 °C in a Beckman Optima ultracentrifuge to remove insoluble material. The protein concentration of the cell lysates was assayed, and the volume was adjusted with RIPA buffer to give 1 mg $ml^{-1}$ protein. For immunoprecipitation, 50 $\mu$l of rabbit anti-$a_3$ antiserum or 2 $\mu$g of anti-$a_1$ rabbit IgG were added to 0.4 ml of cell lysate, which was then incubated at 4 °C for 6 h on a shaking platform. Pre-immune rabbit serum was used as a control. The ImmunoCruz IP/WB Optima B system (Santa Cruz Biotechnology) was used to precipitate antibody-bound proteins where subsequent detection of co-precipitated Ac45 and $A_1$ was performed with mouse antibodies. For detection of $a_1$ and $a_3$, antibody-protein complexes were precipitated by incubation with protein-A/G agarose (Thermo Scientific) for 2 h at 4 °C.

Bead-antibody-protein complexes were recovered by low speed centrifugation, and the pelleted beads were washed three times with RIPA buffer. These were then incubated with SDS-PAGE sample buffer (NuPAGE LDS sample buffer; Life Technologies, Inc.) and heated to 90 °C for 10 min before separation on 4–12 or 10% acrylamide NuPAGE gels (Life Technologies, Inc.). For immunoblotting, protein gels were blotted onto polyvinylidene difluoride membrane and probed with HRP-conjugated goat anti-mouse or anti-rabbit IgG as appropriate. Chemiluminescent signal was captured using a LAS-3000 imaging work station (Fuji Corp., Japan). Exposure times were typically <2 min, with the exception of the $a_4$ antibody where the detectable signal necessitated 20 min of exposure (see Fig. 2, *B* and *E*). The signal from all immunoblots was within the dynamic range of the imaging workstation.

*Extraction of Biotinylated Cell Surface Proteins*—Cells grown on 6-well plates were washed three times with PBS-Mg/Ca and then incubated on ice on a rocking table for 60 min with a solution of 0.2 mg $ml^{-1}$ EZ-Link sulfo-NHS-SS-biotin

(Thermo Scientific) (from fresh 20 mg ml$^{-1}$ stock in DMSO) in PBS-Mg/Ca. Cells were then incubated for 20 min with ice-cold PBS-Mg/Ca containing 100 mM lysine. After aspirating the lysine solution, cells were extracted into RIPA buffer and incubated on ice for 30 min.

To extract a total membrane fraction, cell monolayers from two 175-cm$^2$ tissue culture flasks were recovered by scraping into PBS (supplemented with protease inhibitors), sonicated on ice for 60 s, and centrifuged at $10,000 \times g$ for 20 min at 4 °C. The supernatant was then centrifuged at $100,000 \times g$ for 1 h at 4 °C. The pellet corresponding to a total membrane fraction was resuspended in PBS containing 0.2 mg/ml EZ-Link sulfo-NHS-SS-biotin and incubated on ice for 60 min before addition of lysine (100 mM). The membranes were then recovered by centrifugation at $100,000 \times g$ as above, washed with PBS, and finally resuspended in RIPA buffer before incubation on ice for 30 min.

For recovery of biotinylated proteins, RIPA buffer extracts were centrifuged at $100,000 \times g$ for 20 min and then added to magnetic StrepTactin beads (Qiagen) pre-equilibrated with RIPA buffer. Beads were agitated for 60 min at 4 °C, then recovered using a magnet, followed by two washes with RIPA, one wash with $0.2\times$ RIPA (RIPA buffer with 0.2% w/v Nonidet P-40, 0.1% w/v sodium deoxycholate). The recovered beads were incubated at 90 °C with SDS-PAGE sample buffer, separated by SDS-PAGE, and probed by immunoblotting as above.

To monitor recycling of plasma membrane proteins, cells were cultured, washed, and labeled with sulfo-NHS-SS-biotin as above. After biotinylation and quenching with lysine, control cells (representing a maximally surface-labeled fraction) were removed into RIPA buffer. Internalization of biotinylated surface proteins was initiated by replacing cold PBS-Mg/Ca with HBSS warmed to 37 °C. At 5–120-min time points, residual surface biotin was removed by incubation with 100 mM sodium 2-mercaptoethanesulfonate (MESNa) (in 100 mM NaCl, 1 mM EDTA, 0.2% w/v BSA, 50 mM Tris-HCl, pH 8.6) on ice for 15 min with gentle rocking. MESNa was then quenched by washing with ice-cold 100 mM iodoacetamide in PBS-Mg/Ca. Cells were suspended in ice-cold PBS by aspiration and counted in a hemocytometer. Cells were then recovered by centrifugation ($5000 \times g$, 10 min, 4 °C) and extracted into RIPA buffer with the volume adjusted according to cell count to give an equivalent volume per cell. This suspension was incubated on ice for 30 min. Lysates were centrifuged at $100,000 \times g$ for 20 min (4 °C), and biotinylated proteins within the supernatants were bound to magnetic StrepTactin beads, washed, and analyzed by SDS-PAGE/immunoblotting as above.

*Vesicular pH Assay*—Cells were grown in 24-well plates and incubated with FITC-dextran ((Sigma) 0.5 ml, 0.2 mg ml$^{-1}$) in PBS (with Mg$^{2+}$ and Ca$^{2+}$) for 10 min at 37 °C. Total uptake was determined by washing cells three times with PBS-Mg/Ca at 4 °C, before harvesting by aspiration. Cells were resuspended in PBS with 100 mM KCl and 10 $\mu$M nigericin and placed in a 96-well fluorimeter plate, and the fluorescence was determined in a Cary Eclipse fluorimeter with excitation at 490 nm and emission across the 510–560-nm range. To determine vesicular pH, after washing with PBS-Ca/Mg, cells were incubated with HBSS at 37 °C. At time intervals of 5–60 min, cells were

recovered into PBS and placed in 96-well fluorimeter plate, and the excitation spectrum in the 400–500 nm range was obtained for emission at 520 nm (3 scan average, excitation slit 2.5 nm, emission slit 5 nm, 1200 nm min$^{-1}$ scan speed). The time-dependent change in the ratio of excitation at 492 nm to that at 442 nm for 520-nm emission was then calculated. For calibration, cells were resuspended in PBS, 100 mM KCl, 10 $\mu$g ml$^{-1}$ nigericin with 25 mM MES, 25 mM MOPS with the pH adjusted to 5, 6, 7, or 8 with KOH.

*Fluorescence Microscopy*—For fluorescence microscopy, cells were grown on polylysine-treated coverslips until 70–80% confluent. Coverslips were washed three times with PBS-Ca/Mg before fixing with 4% w/v paraformaldehyde in PBS-Mg/Ca (10 min, room temperature). Paraformaldehyde was quenched by adding NH$_4$Cl to 50 mM in PBS (10 min at room temperature), followed by washing with PBS. Cells were permeabilized with 1% w/v Triton X-100, 1% w/v fish skin gelatin in PBS for 10 min at room temperature, then incubated with 1:250 dilution of anti-$a_3$ polyclonal antiserum or with 5 $\mu$g ml$^{-1}$ purified antibodies for 1 h at room temperature. For MMP-14 labeling, Triton X-100 was omitted. Cells were then washed two times with PBS (20 min each) and then with 1:250 dilution of normal goat serum in PBS. After briefly washing with PBS, Alexa-488-labeled goat anti-rabbit or Texas Red-labeled goat anti-mouse antibodies (Life Technologies, Inc.) were added for 1 h at room temperature, each also containing Hoechst 33258 (1 $\mu$g ml$^{-1}$) for nuclear staining. After washing three times with PBS (20 min each), coverslips were gently blotted and mounted onto slides with Fluoromount G (Southern Biotech), then gently sealed with acrylic, and stored in dark at 4 °C. For controls, primary antibodies were replaced with pre-immune rabbit serum or with purified rabbit or mouse control IgG.

Images were acquired using a DeltaVision deconvolution microscope controlled by the SoftWorx suite of programs at $\times$60 magnification. After locating upper and lower sections of each cell, image stacks in the z-plane were collected typically as 2–3-$\mu$m sections at three excitation/emission settings (for Hoechst 33258, Alexa-488, and Texas Red/Alexa-594). Image acquisition settings (exposure time, filter settings, pixel binning, and excitation power) were kept constant for all images to allow valid comparison and quantitation. Image deconvolution was performed using the corresponding function in SoftWorx. Images of anti-MMP-14 antibody-labeled cells were collected on an EVOS FI inverted digital microscope (Life Technologies, Inc., Paisley, UK).

Pixel coincidence in double-labeled images was quantified using the "co-localization" function of the image analysis software Imaris (Bitplane AG, Zurich, Switzerland). For each channel, background fluorescence was set at 10% of the total signal. Nonspecific binding of control mouse and rabbit IgG and rabbit pre-immune serum were tested but gave negligible signal using the image acquisition settings used consistently for collecting data. Texas Red anti-mouse and Alexa-488-rabbit secondary antibodies were tested, respectively, for their species cross-reactivity to the rabbit ($a_1$ and $a_3$) and mouse (Ac45/TfR/LAMP-1/A) primary antibodies, but again the negligible signal was detected.

**TABLE 1**
Rates of proton extrusion from prostatic carcinoma cells

| Cell type | Medium | ECAR | pH decrease[a] | $J_{H^+, obs}$ | |
|---|---|---|---|---|---|
| | | $\mu V s^{-1}$ | *units* $min^{-1}$ | nM $min^{-1}$ (%) | |
| PC-3 | Na$^+$-HBSS | $320 \pm 40^b$ ($n = 10$) | $0.32 \pm 0.04$ | $43.3 \pm 5.4$ (*100*) | |
| PC-3 | Choline-HBSS | $211 \pm 78$ ($n = 13$) | $0.21 \pm 0.08$ | $28.6 \pm 10.6$ (*66*) | |
| LNCaP | Na$^+$-HBSS | $283 \pm 61^b$ ($n = 9$) | $0.28 \pm 0.06$ | $37.9 \pm 8.3$ (*88*) (*100*) [c] | |
| LNCaP | Choline-HBSS | $184 \pm 52$ ($n = 6$) | $0.18 \pm 0.05$ | $24.4 \pm 7.0$ (*56*) (*64*)[c] | |

[a] Data are from an initial pH of 7.4 (40 nM H$^+$).
[b] $t_{obt} = 1.56$, $p > 0.05$, not different (two-tailed t-test).
[c] Relative rates are for LNCaP cells.

*Transferrin Uptake Assay*—Cells were grown on glass coverslips as above and incubated in serum-free medium for 2 h. Cells were then incubated with Alexa-594-conjugated human transferrin (Molecular Probes, Life Technologies, Inc.) at 25 $\mu$g ml$^{-1}$ on ice for 30 min. As a control, a set of coverslips was also pre-treated with the endocytosis inhibitor Dynasore (80 $\mu$M) for 30 min before exposure to transferrin. Cells were then washed twice with ice-cold PBS-Mg/Ca to remove excess transferrin. "Time 0" cells were immediately fixed for microscopy with paraformaldehyde as above. Transferrin transport was initiated by addition of HBSS warmed to 37 °C, and the cells were moved to an incubator. Coverslips were removed at time points 30–90 min, washed briefly with PBS-Mg/Ca, and processed for microscopy as above, with additional staining for the $a_1$ subunit and with Hoechst 33258. Images were captured using the DeltaVision microscope with fixed acquisition parameters throughout. For each time point, images of 18–30 cells were collected. Quantitation of Alexa-594-tranferrin fluorescence was performed using ImageJ software (rsb.info.nih.gov).

*Gene Expression Profiling*—RNA was isolated from PC-3 cells using RNeasy micro-extraction kit (Qiagen, Germany) and quantified, and the purity was determined by measuring absorbance at 280, 260, and 230 nm using an ND-1000 nanodrop spectrophotometer (LabTech International, UK). After reverse transcription, cDNA was subjected to microarray analysis using the Human Genome U133 Plus 2.0 array (Affymetrix, High Wycombe, UK). Gene expression levels were analyzed using Microarray Suites software. Sequences used in the design of this array were selected from the GenBank$^{TM}$, dbEST, and RefSeq databases.

## Results

*V-ATPase Activity at the Plasma Membrane*—The contribution of the V-ATPase to proton extrusion activity across the plasma membrane of prostatic carcinoma cells (ECAR) was measured by microphysiometry after exposure to concanamycin. Two different PC-3 and LNCaP prostate cell lines were compared for correlation between V-ATPase activity and invasive phenotype. Mean basal rates of H$^+$ pumping across the plasma membrane of PC-3 prostate cells gave a drop in extracellular pH of 0.32 pH units min$^{-1}$, equivalent to a proton pumping rate ($J_H^+$) sufficient to change the proton concentration in the microphysiometer chamber by 43 nM min$^{-1}$ (Table 1). Non-invasive LNCaP prostate cells displayed mean rates that were not significantly different from this (38 nM min$^{-1}$; Table 1). Measurement after infusing with varying concentrations of concanamycin (Fig. 1A) caused a drop in proton extrusion rates ($t_{1/2}$ ~12 min), reversed by washing out the inhibitor

(recovery $t_{1/2}$ ~40 min). For PC-3 cells, the maximal extent of inhibition by concanamycin indicates that $40 \pm 14\%$ of the basal $J_H^+$ is V-ATPase-dependent (Fig. 1B). We found a small but significant difference ($p < 0.05$) in the relative contribution of V-ATPase activity to $J_H^+$ of non-invasive LNCaP cells ($29 \pm 6\%$, Fig. 1B). Infusion with the Na$^+$/H$^+$ exchanger inhibitor ethyl isopropylamiloride at 100 $\mu$M blocked 30 and 34% of $J_H^+$ of PC-3 and LNCaP cells, respectively (Fig. 1B). Similar decreases in $J_H^+$ were observed when measurements were made with nominally sodium-free perfusion medium (Table 1). Although the apparent IC$_{50}$ of 100 nM for concanamycin in both cells types (Fig. 1C) is high compared with published values for *in vitro* effects, such an elevated value is not unexpected for a cell-based assay and is below the concentration at which V-ATPase specificity is lost (52).

Having established that the V-ATPase is a major contributor to proton efflux across the plasma membrane of prostatic carcinoma cells, the relative levels of expression of subunit isoforms that could contribute to this activity were examined by gene array chip analysis (Fig. 2A). In PC-3 prostate cells, isoform B$_2$ with subunit A predominates in the catalytic V$_1$ domain, along with C$_1$, E$_1$, and G$_1$ forms of the stator network subunits. Unexpectedly, the E$_2$ isoform reported to be expressed exclusively in spermatids was also present at relatively high levels (Fig. 2A). Among V$_o$ subunits, the $d_1$ isoform was highly expressed along with the $a_1$ and $a_3$ forms of the large integral membrane component of the V-ATPase stator. The $a_2$ isoform was expressed at low levels, and the $a_4$ kidney-specific isoform was apparently absent. High levels of mRNA transcript encoding subunits D, F, H, *c*, and Ac45 were also detected (Fig. 2A). Note that although comparisons of levels of transcript for unrelated subunits are meaningless, comparisons between isoforms (presumed to have similar transcript length and stability) remain valid.

On the basis that $a_1$ and $a_3$ appeared to be the dominant membrane subunit isoforms, these were examined individually for their localization to the plasma membrane. To validate an assay for plasma membrane expression, surface biotinylation of PC-3 prostate cells with a membrane-impermeable cleavable biotinylation compound (sulfo-NHS-SS-biotin) was tested, followed by pulldown with StrepTactin beads. This generated a fraction that did not contain the late endosome/lysosome marker LAMP-1 and only very low levels of the Golgi marker TGN46 (Fig. 2B). Hence, we concluded that it represented exclusively a plasma membrane-enriched fraction. Only negligible binding of non-biotinylated proteins to the StrepTactin beads was observed. This fraction showed signal on immunob-
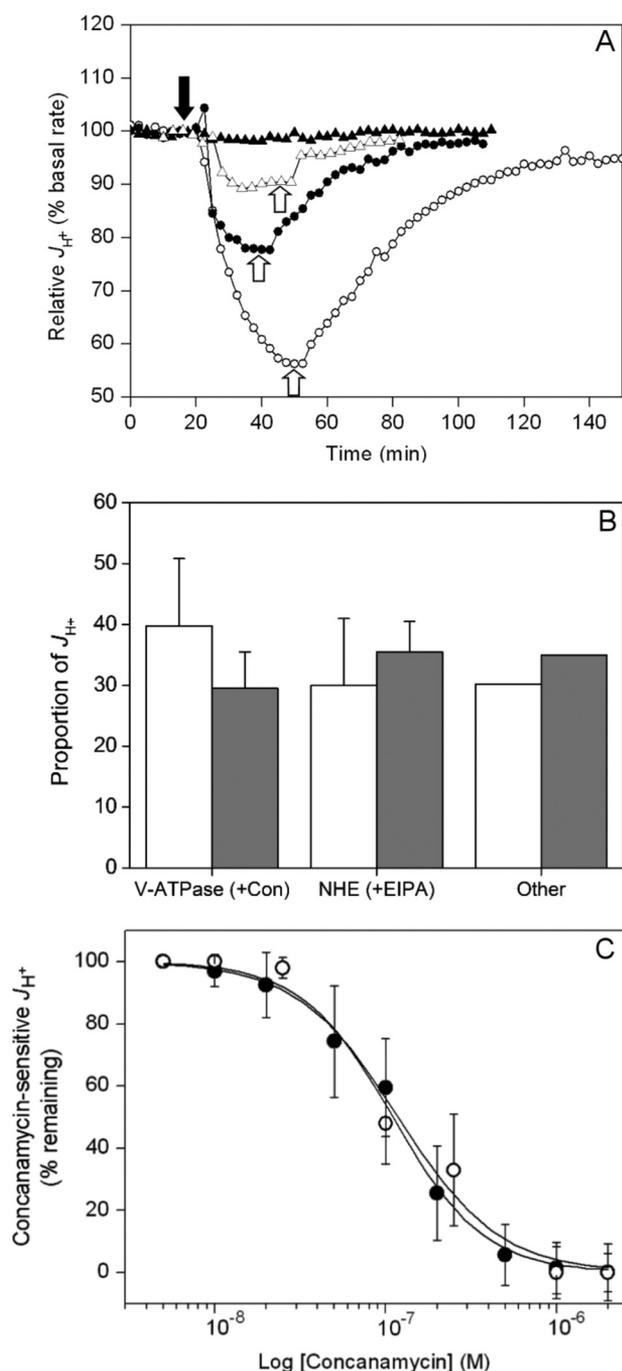
FIGURE 1. **V-ATPase activity at the plasma membrane of prostate carcinoma cells.** *A,* example microphysiometry traces for PC-3 cells. Concanamycin A was added as indicated by the *solid arrow* and washed out at the points indicated by the *open arrows*. *Solid triangles* indicate vehicle only (DMSO); *open triangles* indicate 50 nM; *solid circles* indicate 100 nM; *open circles* indicate 1 μM. *B,* relative contributions of V-ATPase and NHE1 activities to H⁺ extrusion by PC-3 (*white*, $n = 10$ (three readings per measurement)) and LNCaP (*gray*, $n = 6$ (3 cell samples per measurement)) prostatic carcinoma cells were determined as in *A* and expressed as the activity lost after addition of 2 μM concanamycin A (V-ATPase contribution), 50 μM ethyl isopropylamiloride (NHE1 activity), with the residual activity being the sum of other unassigned activities. *Error bars* represent the standard deviation for measurements with each inhibitor (PC-3, $n = 10$; LNCaP, $n = 6$). Differences between relative V-ATPase contributions to $J_{H^+}$ in the two cells types are not statistically significant ($p = 0.055$, unpaired *t* test). *C,* inhibition curves for the concanamycin-sensitive component of $J_{H^+}$ of PC-3 (*solid circles*) and LNCaP cells (*open circles*). Values are expressed as the percentage of the concanamycin-sensitive activity in *B* remaining after inhibitor addition. *Error bars* represent standard deviation of each measurement ($n = 4$). $EC_{50}$ for both cells lines is ~100 nM.

lots for both $a_1$ and $a_3$, along with $V_1$ subunit A and Ac45 (Fig. 2*B*). Isoform $a_1$ was detected with an antibody recognizing residues 71–210 (that has 32% identity with the corresponding part of $a_3$) and $a_3$ with an antibody raised against a peptide of residues 689–707 (11% identity to the corresponding $a_1$ region) (53). Contrary to the expression data, the $a_4$ isoform was also detectable in the total membrane fraction after long exposure of the chemiluminescent immunoblot. It was not detectable in the plasma membrane fraction when the protein loaded on the immunoblot was equivalent to that in the other lanes in Fig. 2*B*, but it was detectable at higher loading (discussed below). We were not able to detect the $a_2$ isoform by immunoblot in either total membrane or plasma membrane fractions (data not shown). These data indicate that both $a_1$ and $a_3$ V-ATPase isoforms are simultaneously present at the plasma membrane of PC-3 cells.

To investigate isoform contributions to V-ATPase-dependent proton extrusion, we established the conditions needed for knockdown of V-ATPase subunit expression by RNA interference (RNAi) using synthetic inhibitory RNA (siRNA) oligonucleotides. Pools of siRNAs and their four constituent siRNAs were tested for effects on protein expression, along with a negative control version of one of the constituent siRNAs from each pool (see "Experimental Procedures"). Although relatively high siRNA concentrations (100 nM) and long transfection times (24 h) were required, ~80% reduction in levels of $a_1$ and $a_3$ was achieved as judged by immunoblotting (Fig. 2*C*). Ac45 (ATP6AP1) has been implicated in V-ATPase accumulation at the plasma membrane of neuroendocrine cells (49) and in directing the V-ATPase to the ruffled membrane of activated osteoclasts, a specialized region of the plasma membrane (48). In PC-3 prostate cells, Ac45 is not only present at relatively high levels but also localized to the plasma membrane (Fig. 2*B*). To examine the role of Ac45 in V-ATPase trafficking, Ac45 was also subjected to RNAi knockdown, and the impact of this on different V-ATPase functions was measured. Treatment with 25 nM siRNA for 24–48 h gave >90% depletion of Ac45 levels (Fig. 2*C*). For $a_1$, $a_3$, and Ac45, treatment with a negative control mutant version of an siRNA from each pool resulted in no significant loss of expression (Fig. 2*C*), underlining the specificity of the expression knockdown. Depletion of subunit A expression by >90% was also achieved after 24 h with 25 nM of an siRNA pool (Fig. 2*D*).

Overall levels of $a_1$ and $a_3$ in the total membrane fraction were not affected by subunit A knockdown (Fig. 2*D*), indicating that $V_o$ stability is not dependent on subunit A. Loss of subunit F however implies complete disruption of $V_1$ assembly. In a mouse knock-out model, up-regulation of the $B_2$ subunit can compensate for loss of $B_1$ (54), with some functional compensation also possible between the subunit $a$ homologues Vph1p and Stv1p in *Saccharomyces* (55). Here, knockdown of either $a_1$ or $a_3$ did not result in a corresponding increase in the levels of the other isoform at the plasma membrane (Fig. 2*E*), suggesting no compensatory mechanism. With 10-fold higher loading than in Fig. 2*B* and long exposure, some signal for the $a_4$ isoform was also detected, but levels were similarly unaffected by knockdown of either $a_1$ or $a_3$. Depletion of these subunit isoforms did result in a decrease in the signal from subunit A
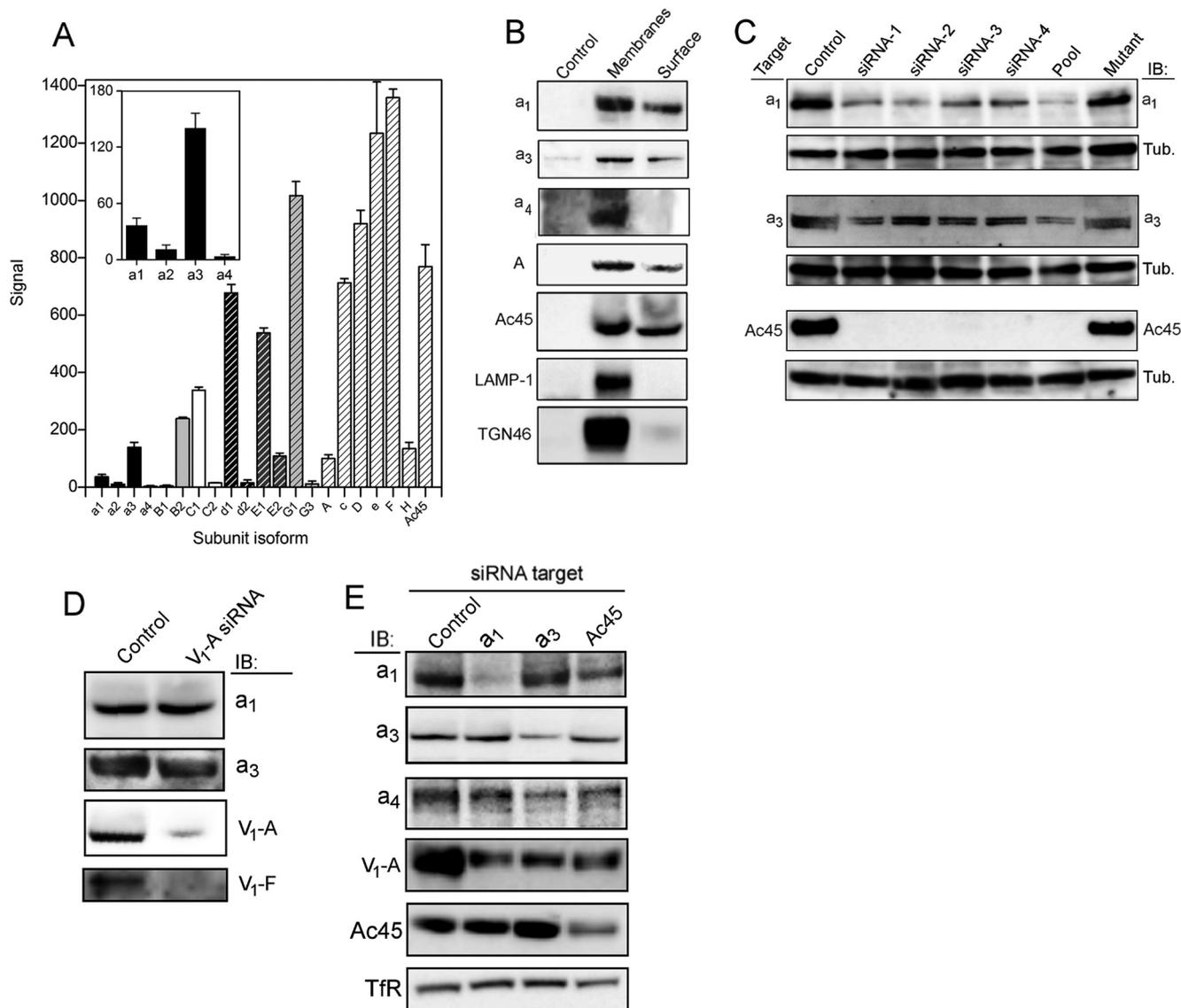
FIGURE 2. **Expression of V-ATPase subunit isoforms in PC-3 cells.** *A,* extracted mRNA from PC-3 cells was reverse-transcribed and analyzed on Affymetrix DNA microarrays (see "Experimental Procedures"). Mean values were determined from the output of two independent analyses. *Columns* indicating isoforms of a particular subunit have *equivalent shading*. Subunits represented on the array by only a single gene (A, c, D, e, F, H and Ac45) have the *same shading*. Output for the ATP6V0A1–4 genes is magnified in *inset*. *B,* to detect proteins accessible to the extracellular medium, intact PC-3 cells were labeled with membrane-impermeable biotinylation reagent prior to solubilization and extraction with StrepTactin affinity beads, followed by immunoblot analysis (*Surface*). As a control for reactivity, a detergent-solubilized membrane fraction was subjected to the same analysis (*Membranes*). Non-biotinylated protein gave negligible binding to the StrepTactin resin (*Control*). The Membranes samples contain 20 $\mu$g of total protein with the exception of the $a_4$ blot, which contains 50 $\mu$g. Surface sample loading is the same in each blot, adjusted to give equivalent intensity in membranes and surface for Ac45. Chemiluminescence capture for $a_4$ was 10-fold longer than for the other immunoblots. *C,* knockdown of $a_1$, $a_3$, and Ac45 expression by RNAi. PC-3 cell lysates (15 $\mu$g of protein) were analyzed by immunoblotting (*IB*) with the corresponding subunit-specific antibody after transfection with isoform-specific siRNAs. Tubulin (*Tub.*) levels were used to ensure equivalent loading. Individual siRNAs that make up each Dharmacon SmartPool were individually tested (*siRNA1–4*), along with the corresponding pool (*Pool*). A version of siRNA-1 synthesized to include nucleotide changes as set out under "Experimental Procedures" was also tested (*Mutant*). *D,* RNAi knockdown of subunit A disrupts $V_1$ assembly but does not affect subunit *a* expression. A total membrane fraction was isolated from cells after transfection with an siRNA pool specific for ATP6V1A. Lanes were loaded with 30 $\mu$g of total protein and immunoblotted (*IB*) for $V_o$ subunits $a_1$ and $a_3$ and $V_1$ subunits A and F. *E,* effects of siRNA knockdown on levels of non-targeted subunits at the plasma membrane. Cell surface proteins were extracted after biotinylation as in *B* from cells transfected with siRNAs for $a_1$, $a_3$, and Ac45. Biotinylated extract from $1 \times 10^5$ cells ($5 \times 10^5$ for subunit $a_4$) were analyzed by immunoblot (*IB*) for $a_{1/3/4}$, subunit A, and Ac45. TfR was used as a loading control. Data capture for the $a_4$ immunoblot was for 10× longer than for the other samples.

associated with the plasma membrane fraction, consistent with decreased assembly due to reduced availability of $V_o$. Ac45 knockdown had a similar effect on subunit A and $a_1$ levels (but no reproducible effect on $a_3$) (Fig. 2*E*), consistent with a role for the accessory subunit in V-ATPase delivery to the cell surface.

*Intracellular Localization of V-ATPase Subunit Isoforms—* An investigation of the intracellular distribution of the V-ATPase $a_1$ and $a_3$ subunits by immunofluorescence micros-

copy revealed distribution in different (but in part overlapping) compartments (Fig. 3). Staining for the $a_1$ isoform was punctate (consistent with its presence in small vesicles) and distributed throughout the cytoplasm (Fig. 3, *A–C*). This staining was coincident with that of TfR (CD71), a marker for the plasma membrane and early endosomes (Fig. 3*B*), but not with the late endosome/lysosome marker LAMP-1 (Fig. 3*A*). The converse situation was observed with the $a_3$ isoform; it showed much
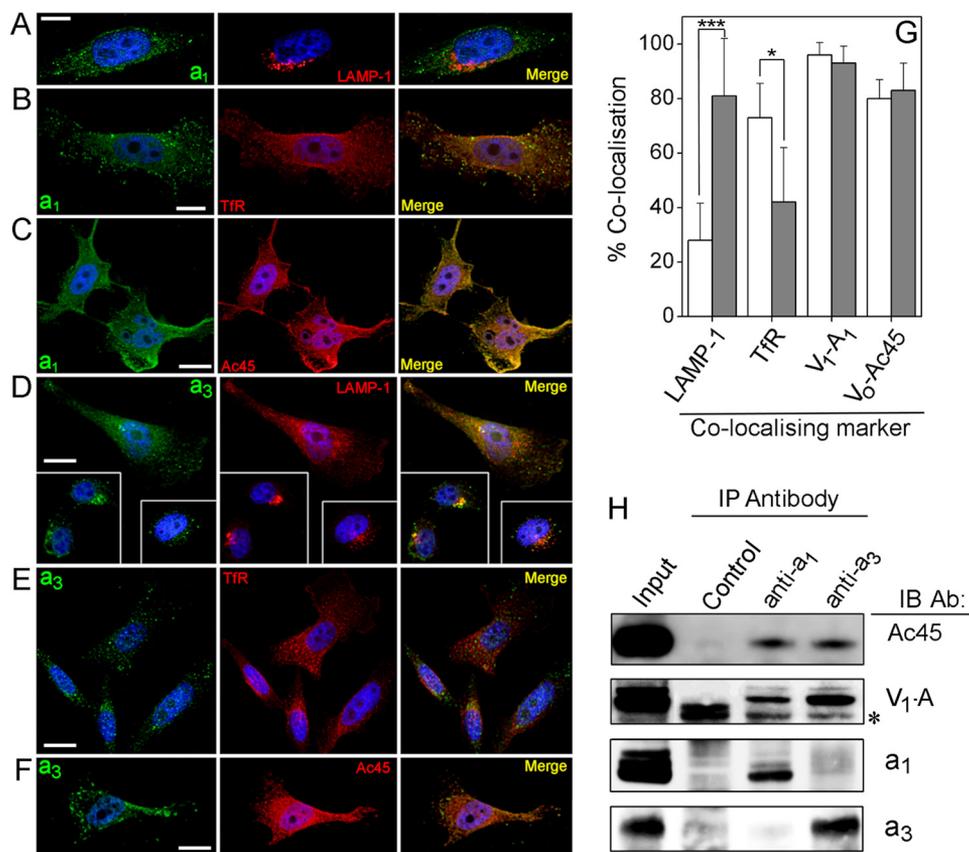
FIGURE 3. **Subcellular localization of the $a_1$ and $a_3$ subunits.** *A–F,* immunofluorescence microscopy of fixed and permeabilized PC-3 cells. *Left column,* cells stained with antibodies to $a_1$ (*A–C*) or $a_3$ (*D–F*). *Center column,* staining with antibodies to LAMP-1 (*A* and *D*), TfR (*B* and *E*), or Ac45 (*C* and *F*). *Right column,* merged images of those in *left* and *center columns*, with coincident pixels colored *yellow*. Nuclei are stained with Hoechst 33258. *Scale bars,* 10 $\mu$m (*A* and *B*) or 20 $\mu$m (*C–F*). *G,* quantitation of co-incident staining. Images such as those in *A–F* were analyzed using the Coincidence function of Imaris software. Values are expressed as the percentage of pixels showing staining for $a_1$ (*open histograms*) or $a_3$ (*gray histograms*) that also stain for the subcellular marker indicated. *Error bars* represent standard deviation. The $a_3$ isoform showed significantly greater ($p < 0.01$) co-localization with the late endosomal marker LAMP-1 (38 cells analyzed) than did $a_1$ (26 cells analyzed), $a_1$ co-localizing significantly more than $a_3$ ($p < 0.05$) with the plasma membrane/endosome marker TfR (23 and 27 cells, respectively). Both $a_1$ and $a_3$ showed strong co-localization with subunit A and Ac45 (11–24 cells analyzed). *, $p < 0.01$; ***, $p < 0.001$. *H,* both $a_1$ and $a_3$ associate with Ac45. The $a_1$ and $a_3$ subunit isoforms were immunoprecipitated (*IP*) from detergent-solubilized PC-3 cell lysate, and co-precipitating proteins were analyzed by immunoblotting (*IB*). Precipitation with normal rabbit serum was used as a control for nonspecific binding. A sample containing the equivalent amount of cell lysate to that used in the immunoprecipitations was also run (*Input*). In the immunoblot of the A subunit, the *asterisk* indicates recognition of the heavy chain of the precipitating IgG. *Ab,* antibody.

greater coincidence with LAMP-1 than with TfR (Fig. 3, *D* and *E*). Both $a_1$ and $a_3$ showed substantial co-distribution with Ac45 and A (Fig. 3, *C* and *F*). Quantification of pixel co-distribution in merged optical sections (Fig. 3, *A–F*) confirmed that $a_1$ predominantly co-localizes with TfR-enriched early endosomes, whereas $a_3$ is predominantly associated with LAMP-1-containing late endosomes/lysosomes (Fig. 3*G*). Both $a_1$ and $a_3$ showed ~95% co-distribution with A, suggesting relatively little V$_o$ detached from V$_1$, and ~80% co-distribution with Ac45, suggesting that the majority of V-ATPases with either subunit *a* isoform associates with this accessory subunit. On the basis of these data, it appears that $a_1$ and $a_3$ exist largely in different compartments of the endocytotic machinery, albeit with some degree of overlap. Immunoprecipitation of detergent-solubilized V-ATPase complexes (Fig. 3*H*) showed that antibodies to either $a_1$ or $a_3$ isoforms co-precipitated Ac45 and A subunits. Precipitates generated by pulldown with either anti-$a$ antibody gave no signal on immunoblots probed with the antibody to the other isoform (Fig. 3*H*), confirming that the respective antibody probes were highly isoform-specific.

*Functional Effects of RNAi Knockdown of V-ATPase Subunits—*Although PC-3 cells transfected with a non-targeting control siRNA pool and with mutant versions of individual siRNAs proliferated at essentially normal rates (doubling time of ~48 h), cultures of cells depleted for V-ATPase subunits were essentially static (Fig. 4*A*). The transfected cells did however remain alive (as judged by calcein-AM uptake), with no appreciable differences in the proportion of dead cells between control and V-ATPase-depleted cultures (4–5%; Fig. 4*A*). Cessation of growth after V-ATPase knockdown serves to underline the importance of its function in cell physiology.

The effects of RNAi knockdown of $a_1$/$a_3$ levels on the invasive properties of PC-3 cells were also tested by measuring chemotactic migration through an extracellular matrix extract (Matrigel) (Fig. 4*C*). Knockdown of either $a_1$ or $a_3$ by individual or pooled siRNAs strongly suppressed migration in this model of metastatic potential, clearly indicating that both isoforms make significant contributions to the invasive phenotype of PC-3 cells. Mutations to inhibitory siRNAs from both $a_1$ and $a_3$ pools that permitted normal levels of expression also led to cells
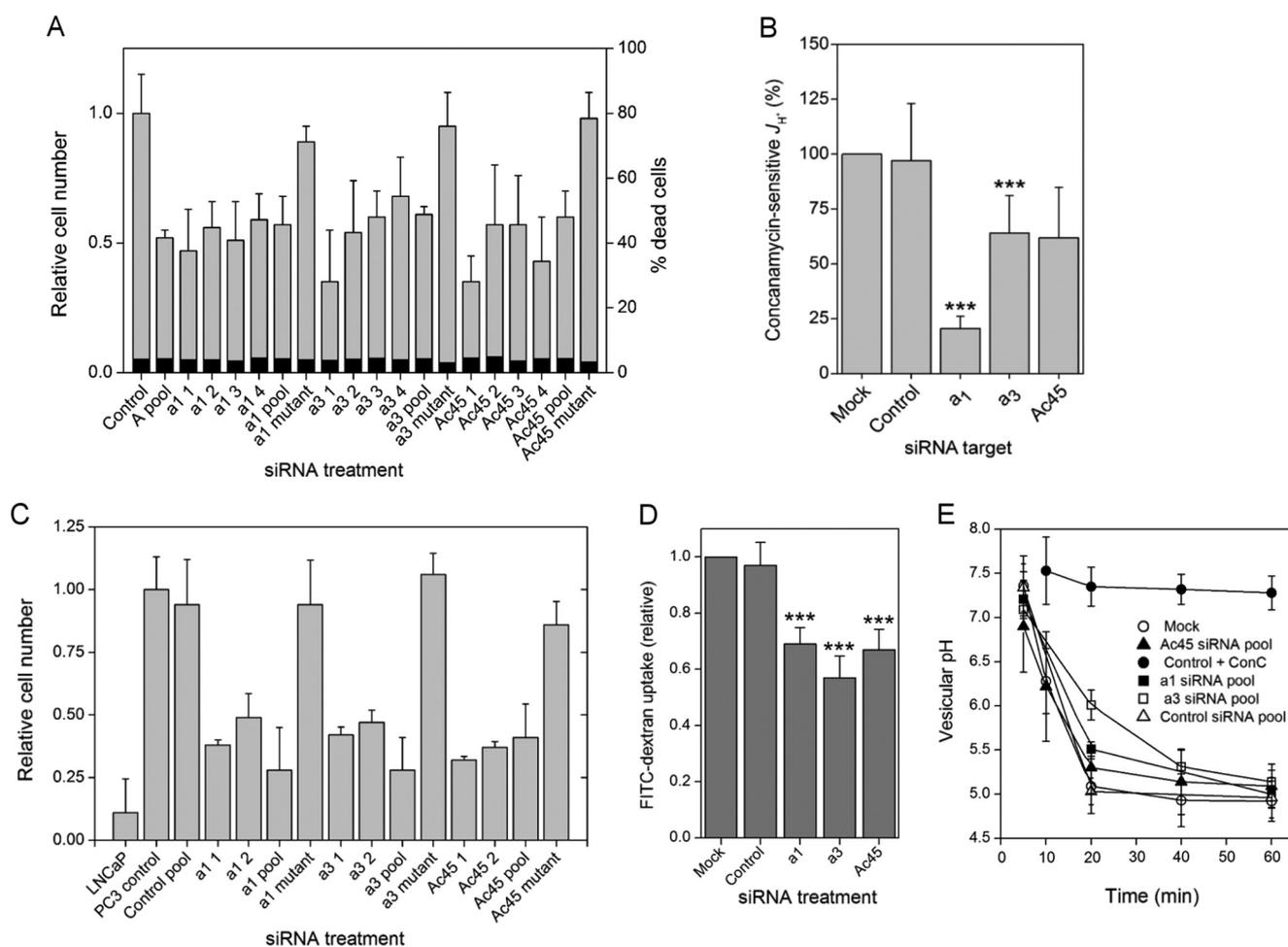
FIGURE 4. **Effects of siRNA knockdown on V-ATPase function in PC-3 cells.** *A,* assay of live/dead cells after siRNA treatment. As in Fig. 1, individual siRNAs that make up each pool were individually tested (*siRNA1–4*), along with the corresponding pooled siRNAs and mutant version. Numbers of viable cells 48 h after siRNA transfection were measured by calcein fluorescence and expressed relative to the change in number of cells in a control transfected with non-targeting siRNA. Numbers of dead cells (as a percentage of the total) were measured by propidium iodide uptake (measurements made in duplicate or triplicate in 96-well format, repeated 4 times). *B,* effect of non-targeting (*control*) and $a_1$, $a_3$, and Ac45-specific siRNAs on concanamycin-sensitive $H^+$ efflux. The concanamycin-sensitive activity remaining after siRNA treatment was determined by adding the compound (2 $\mu$M) and expressed relative to the activity in control cells (equivalent to the concanamycin-sensitive activity shown in Fig. 1*B*). *Error bars* indicate standard deviation of each measurement ($n = 3$, two cell samples per measurement). Both $a_1$ and $a_3$ siRNAs significantly decreased the concanamycin-sensitive component of $J_H^+$ ($a_1$, $p < 0.01$; $a_3$, $p < 0.05$). *C,* $a_1$, $a_3$, and Ac45 siRNAs suppress the invasive phenotype of PC-3 cells. PC-3 cells were induced to migrate through Matrigel using FBS as chemoattractant. Cells treated with siRNAs (two individual siRNAs from each pool, the complete four siRNA pool and a mutant version (detailed under "Experimental Procedures")) were used 24 h post-transfection. Cells migrating through the Matrigel layer were counted after 24 h, and numbers were expressed relative to the untreated PC-3 cell control. Invasiveness of mock-transfected cells (*Control pool*) was not significantly different from untreated cells. PC-3 cells were significantly more invasive than a non-invasive LNCaP control ($p < 0.001$), and $a_1$, $a_3$, and Ac45 siRNAs (individual or pooled) all showed significantly decreased cell invasiveness ($p < 0.01$; $n = 3$, with three replicates per determination). *D* and *E,* uptake of FITC-dextran and measurement of vesicular pH. *D,* total uptake after 10 min measured as the fluorescence emission at 520 nm for cells treated with siRNAs that were non-targeting pool (*Control*) or pools targeted to Ac45, $a_1$, or $a_3$ subunits. *Error bars* show standard deviation ($n = 3$). All targeting siRNAs caused significant effects (***, $p < 0.001$). *E,* change in the vesicular pH experienced by the endocytosed FITC-dextran, measured as the change in the 492 nm/442 nm excitation ratio for emission at 520 nm. *Open circles,* untreated cells; *closed circles,* 2 $\mu$M concanamycin; *open triangles,* control (non-targeting) siRNA; *closed triangles,* Ac45 siRNA. *Closed* and *open squares,* $a_1$ and $a_3$ siRNAs, respectively. *Error bars* indicate standard deviation ($n = 3$).

achieving normal levels of invasiveness (Fig. 4*C*), further indicating the specificity of the RNAi effect.

Loss of invasiveness of breast cancer cells after $a_3$ knockdown has previously been reported, with effects similar to those caused by treatment with bafilomycin A1 (33). It is unclear whether these effects are mediated via a decrease specifically in $J_H^+$ or through broader cellular effects such as arrest of trafficking. Pertaining to this, we have observed that the cytokine receptor activator of nuclear factor $\kappa$B ligand has no effect on $J_H^+$, but the ~50% increase in invasiveness it causes is completely ablated by concanamycin A (data not shown). Receptor activator of nuclear factor $\kappa$B ligand is

reported to increase invasiveness of prostate and breast cancer cells of epithelial origin via c-Src and MAPK signaling pathways (56, 57). As discussed below, knockdown of $a_3$ in particular affects invasion to a much greater extent than it does $J_H^+$ (Fig. 4*B*). Consequently, it is likely that the effects of $a_1$ and $a_3$ knockdown are mediated via changes to trafficking processes in the cell rather than to decreased acidification of the extracellular environment.

Ac45 depletion by siRNA pool and by individual RNAs also significantly decreased PC-3 cell invasiveness *in vitro*, although invasiveness was unaffected by a mutant version of representative siRNA (Fig. 4*C*). This points to a role for Ac45 in navigating

both V-ATPase isoforms around the cell, a phenomenon we investigated further in this study.

Knockdown of $a_1$ levels eliminated $78 \pm 6\%$ of the concanamycin-sensitive component of $J_H^+$, whereas depletion of $a_3$ levels accounted for only $34 \pm 17\%$ (Fig. 4*B*), indicating that it is predominantly an $a_1$-containing V-ATPase that contributes to $J_H^+$ in these cells, with an $a_3$ isoform making a much smaller (but significant) contribution to this activity. Because efficiency of RNAi knockdown of each isoform is broadly equivalent (Fig. 2*C*), the data in Fig. 4*B* suggest an $\sim$2:1 split in the contribution of the two isoforms to the bafilomycin-sensitive $J_H^+$ component. We note however that the sum of effects of even incomplete $a_1$ or $a_3$ knockdown on plasma membrane V-ATPase activity is >100% inhibition, implying that $a_3$ knockdown has some influence on plasma membrane activity of the $a_1$-containing isoform and vice versa. This is not unexpected given the dynamic inter-relationship between membrane compartments within the cell. Depletion of Ac45 also caused a trend toward loss of concanamycin-sensitive $J_H^+$, but these measurements were prone to high variance and hence the trend indicating 40% loss of activity was not significant at the 95% confidence limit (Fig. 4*B*).

Fluid-phase endocytosis was significantly reduced after Ac45, $a_1$, or $a_3$ knockdown as indicated by a decreased uptake of FITC-labeled dextran (Fig. 4*D*). However, neither the rate of endosomal/lysosomal vesicular acidification nor the final minimum pH levels experienced by the dextran in vesicles were significantly different from controls when $a_1$ or Ac45 was depleted by siRNA transfection (Fig. 4*E*). Only $a_3$ knockdown appeared to have any effect on this process, initially slowing the rate at which the pH of FITC-dextran-loaded vesicles decreased, but ultimately with no significant effect on the minimal pH achieved.

*Requirement for V-ATPase Subunits in Endocytosis and Trafficking*—Substantial co-distribution of $a_1$ with TfR implies that they move together through the endosomal recycling system. To examine this, we tested the impact of siRNA depletion of $a_1$ and $a_3$ on TfR (CD71) recycling using a surface biotinylation protection assay. This involves membrane protein biotinylation (on ice) of extracellular surface-exposed amine groups with a membrane-impermeable but reversible (disulfide-containing) reagent, followed by resumption of endocytosis by incubation at 37 °C. Biotinylated membrane protein internalization prevents removal of the biotin moiety by incubation with a water-soluble reductant (MESNa); hence, pulldown of the total biotinylated fraction from cell lysates reports on the kinetics of endocytosis. For control cells, biotin removal indicative of TfR re-exposure at the cell surface occurred with a half-time of $\sim$45 min (Fig. 5, *A* and *B*). Transfection with siRNAs targeted against the $a_1$, $a_3$, Ac45 (pooled or individual siRNAs), or A soluble domain subunits had no significant effect on the initial internalization, with broadly equivalent levels of internalized TfR consistently seen up to 30 min after restart of endocytosis (Fig. 5, *A–C*). However, knockdown of $a_1$ and Ac45 significantly slowed the rate of biotin removal from TfR, with levels of receptor biotinylation remaining essentially constant across the 120-min time course, indicating retention of the receptor inside the cell. Treatment with an $a_3$-depleting siRNA

pool caused some slowing of TfR recycling, an individual siRNA from that pool actually having a more clearly defined effect (Fig. 5, *A* and *B*). Depletion of $a_1$ and Ac45 (and less conclusively $a_3$) therefore significantly slowed transit of TfR through the endosomal recycling system. Because of the non-catalytic role of $V_o$ in membrane fusion (58, 59), the observed effect could be due either to loss of acidification or to inhibition of membrane fusion events. Because membrane fusion should not be affected by loss of V-ATPase catalytic activity, effects resulting from RNAi knockdown of the catalytic subunit A can discriminate between these possible mechanisms. Subunit A depletion (Fig. 5*A*) stalled TfR recycling in a similar way to $a_1$ knockdown without affecting levels of $a_1$ in the membrane (Fig. 2*D*), and it was indistinguishable from the effect of directly inhibiting proton pumping with bafilomycin A1 (Fig. 5, *A* and *C*). Arrest of TfR recycling by $a_1$ depletion is likely to be mediated via altered vesicular acidification and not by direct effects on membrane fusion. The siRNA effects appeared to be highly specific, with mutant versions of expression-suppressing siRNAs having no significant effects on TfR recycling.

The impact of Ac45 depletion on plasma membrane protein recycling was further resolved using the surface biotinylation assay. In control cells, TfR was internalized with a $t_{1/2}$ of $\sim$15 min (Fig. 5, *D* and *E*), with loss of biotinylation after $\sim$2 h consistent with recycling back to the cell surface (or degradation). Knockdown of Ac45 elicited a major change in uptake kinetics; TfR internalization was slowed, with a $t_{1/2}$ of $\sim$45 min; recycling of TfR back to the plasma membrane could not be detected even after 2 h (Fig. 5, *D* and *E*). A similar change in the dynamics of subunit $a_1$ internalization and recycling was also observed (Fig. 5, *D* and *E*). Maximal $a_1$ internalization in Ac45-depleted cells occurred after >2 h compared with $\sim$30 min in control cells. These data indicate that the $a_1$-containing V-ATPase, although active at the plasma membrane, is endocytosed relatively quickly in an Ac45-dependent manner.

The observed effect of Ac45 depletion on membrane cycling to the cell surface could also impact the delivery/secretion of ECM-degrading enzymes, offering an explanation for the impact of Ac45 knockdown on PC-3 cell invasiveness *in vitro* (Fig. 4*C*). To examine this further, we looked at the effect of Ac45 depletion on delivery of the membrane-bound matrix metalloprotease MMP-14 to the cell surface. Highly expressed at the plasma membrane of cancer cells (60), MMP-14 activates collagenases leading to degradation of the ECM and is specifically linked to cell invasiveness (61, 62). Here, using immunofluorescence labeling of non-permeabilized cells with an antibody recognizing the extracellular region of MMP-14 (Fig. 5, *F* and *G*), Ac45 depletion caused a significant decrease in antibody-accessible protein at the cell surface (Fig. 5*H*). Disturbance of V-ATPase dynamics through loss of Ac45 therefore not only impacts the ability of the cell to sustain a low extracellular pH (Fig. 4*B*) but also its ability to secrete ECM degrading activities. Both are important factors in expression of the invasive phenotype.

The effects of V-ATPase subunit depletion on transit through the endosome-lysosome system were also monitored by following time-dependent changes in the intracellular distribution and total fluorescence signal of Alexa-594-Tf as a proxy
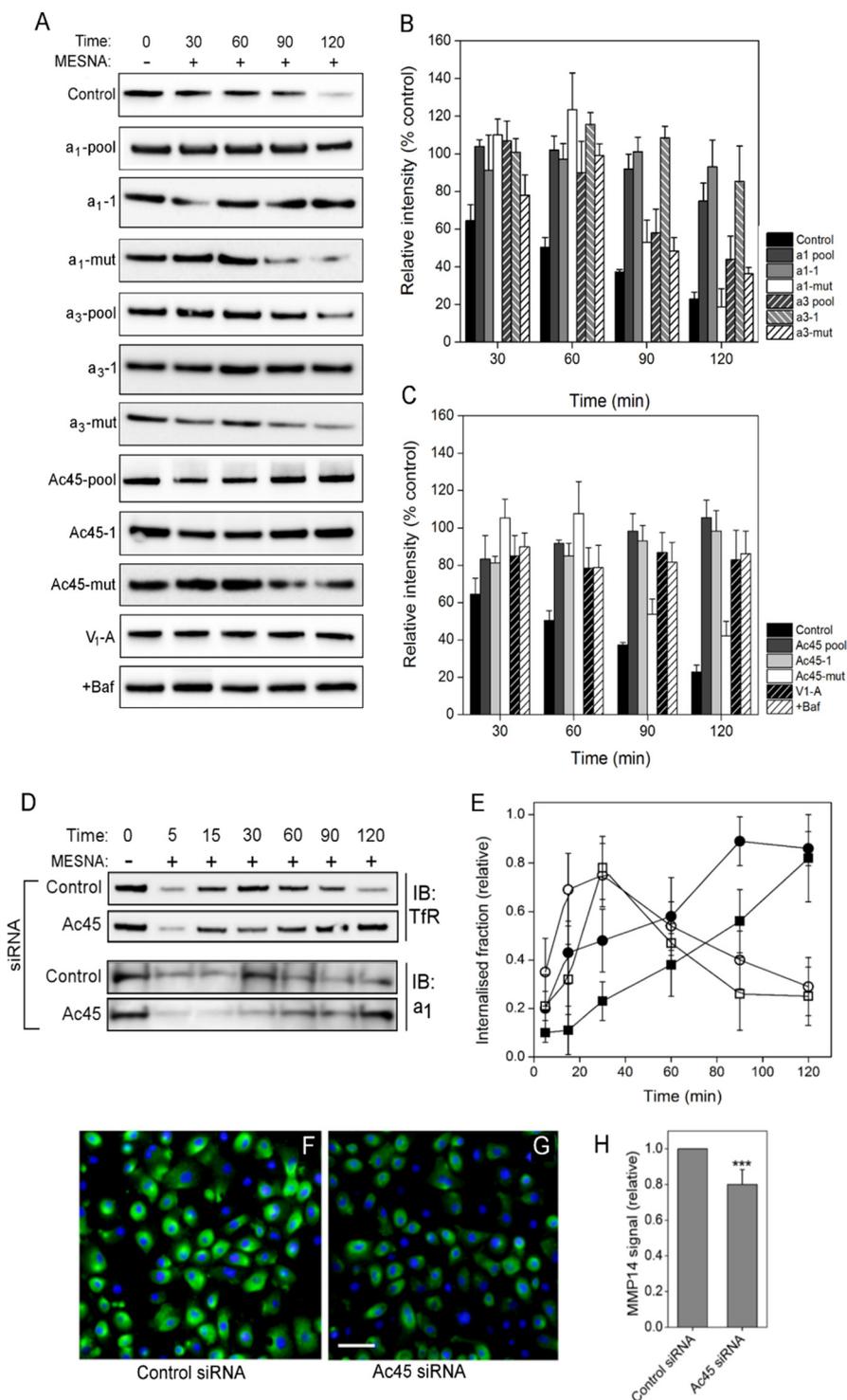
FIGURE 5. **Effects of subunit $a_1$, $a_3$, and Ac45 depletion on TfR recycling dynamics.** *A,* recycling of the TfR was monitored using the surface biotinylation assay as under "Experimental Procedures" in cells treated with non-targeting siRNA pool (*Control*); siRNA pools targeted to $a_1$, $a_3$, Ac45 ($a_1/a_3/Ac45$-*pool*); representative individual siRNAs from each pool ($a_1/a_3/Ac45$-*1*); and the corresponding mutant version of that siRNA ($a_1/a_3/Ac45$-*mut*). To monitor the effects of disruption of proton pumping, cells were treated with an siRNA pool targeted to subunit A (*V1-A*) or pre-treated for 30 min with 100 nM bafilomycin A1 (+*Baf*). After stripping residual surface biotinylation with MESNa, internalized biotinylated proteins were extracted from solubilized cells by binding to StrepTactin beads. Internalized TfR retaining biotin was detected by immunoblotting. *B* and *C*, quantitation of immunoblots as in *A* by densitometry. Values are expressed as a proportion (%) of the maximally biotinylated state at time 0. *Error bars* indicate standard deviation of the mean value (*Control, n* = 3). *D,* Ac45 depletion arrests recycling of plasma membrane proteins. Recycling of the transferrin receptor (*TfR*) and the $a_1$ isoform was monitored after siRNA knockdown of Ac45 using a surface biotinylation assay as above. At the specified time points, biotinylated proteins were extracted by binding to StrepTactin beads. Bound proteins were analyzed by immunoblotting, typical examples being shown for transferrin receptor (*D, upper panel*) and $a_1$ (*D, lower panel*). *E,* quantitation of immunoblots by densitometry. *Open symbols,* cells treated with control (non-targeting) siRNA. *Closed symbols,* treated with Ac45 siRNA. Values are expressed as a proportion of the maximally biotinylated state at time 0. *Error bars* indicate standard deviation (TfR, *n* = 5; $a_1$, *n* = 3). *F–H*, Ac45 depletion decreases cell surface expression of MMP-14. Sample immunofluorescence images of non-permeabilized control (*F*) or Ac45 siRNA-transfected (*G*) PC-3 cells labeled with an antibody recognizing the extracellular domain of MMP-14. Nuclei are stained with Hoechst 33258. *Scale bar,* 20 $\mu$m. *H,* quantitation of the labeling in control and Ac45-depleted cells. Fluorescence from raw images (15 random fields containing ~100 cells from three separate experiments) was quantified using ImageJ. ***, *p* < 0.001.
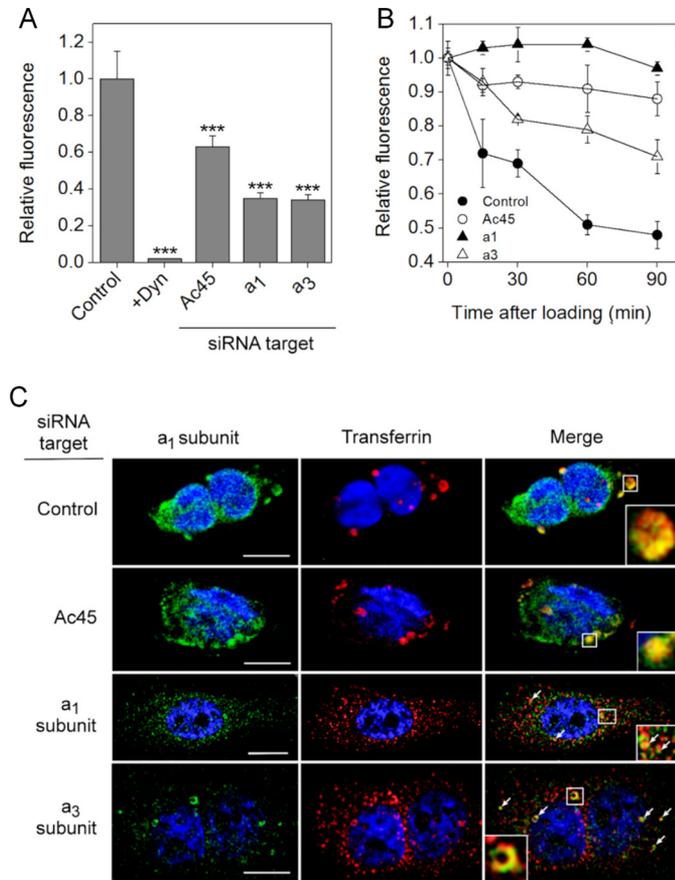
FIGURE 6. **Effects of Ac45 expression knockdown on endocytosis of transferrin.** *A,* Alexa-594-Tf uptake by PC-3 cells treated with control (non-targeting), Ac45, $a_1$- or $a_3$-targeted siRNA pools. As negative control, cells were also treated with the endocytosis inhibitor dynasore (*Dyn*). After washing off excess transferrin, cells were fixed for microscopy, and the fluorescence from raw images was determined (10–25 images) using ImageJ software. All treatments resulted in significant ($p < 0.01$) loss of transferrin uptake. ***, $p < 0.01$. *B,* time-dependent changes in Alexa-594-Tf fluorescence in siRNA treated cells. After the initial transferrin loading, cells were returned to 37 °C before fixing at different time points. Alexa-594-Tf fluorescence was determined as in *A.* *Closed circles,* control (non-targeting) siRNA pool; *open circles,* Ac45 siRNA pool; *closed triangles,* $a_1$ siRNA pool; *open triangles,* $a_3$ siRNA pool. On average, 20 images were captured and quantified for each time point for each siRNA treatment. *C,* immunofluorescence microscopy of fixed and permeabilized siRNA-treated cells 90 min after initiation of Alexa-594-Tf uptake, stained for the $a_1$ subunit (FITC, *left column*). *Center column,* Alexa-594-Tf fluorescence. *Right column,* merged images with coincident pixels colored *yellow*. *Insets* and *arrows,* details of vesicular structures showing coincident fluorescence. Contrast has been adjusted to highlight qualitative aspects, but quantitation was performed on raw images captured using constant microscope parameters. Nuclei are stained with Hoechst 33258. *Scale bar,* 20 $\mu$m.

for its receptor, TfR (Fig. 6). After initial binding of labeled Tf ligand for 30 min at 4 °C, cells showed characteristic labeling of the cell periphery that was qualitatively similar regardless of siRNA applied. Quantitatively, Ac45 knockdown decreased Tf uptake by ~40% (Fig. 6A), with an even greater effect observed upon knockdown of $a_1$ (65% decrease) or $a_3$ (64% decrease). Treatment of control cells with the pharmacological dynamin inhibitor "dynasore" (63) almost completely abolished Tf endocytosis (Fig. 6A). Monitoring Alexa-594-Tf fluorescence over time allowed Tf recycling and release from the cell to be monitored (Fig. 6B). In control cells, ~54% of the signal was lost over a 90-min period. However, knockdown of Ac45 or $a_1$ levels caused the Alexa-594-Tf signal to decrease by no more than

12% over this period, consistent with retention of the labeled Tf in the endosomal system. Depletion of $a_3$ in the cell also appeared to slow Tf recycling, although this effect was not as pronounced as in Ac45/$a_1$-depleted cells. In control cells, internalized transferrin co-localized with $a_1$ in large perinuclear vesicular bodies (Fig. 6C, *row 1*), qualitatively similar to previous observations (64) and presumed to be recycling endosomes. Cells in which Ac45 was depleted showed qualitatively similar distribution of large Tf/$a_1$-containing vesicles (Fig. 6C, *row 2*). This infers that although transferrin uptake is decreased as a result of Ac45 depletion (as shown in Fig. 6A) because TfR is retained in the cell (Fig. 5, *D* and *E*), the endocytosed Tf ultimately ends up in the same compartment as in control cells. The key difference is that in the absence of Ac45, the large vesicular bodies in which Tf accumulates recycle only very slowly back to the cell surface. Hence, the effects of Ac45 knockdown appear to inhibit both internalization from the plasma membrane and transit back to the cell surface.

Although the effects of depleting either subunit $a$ isoform showed broadly similar effects to Ac45 depletion by inhibiting Tf endocytosis (Fig. 6A) and accumulation within intracellular compartments (Fig. 6B), there were marked differences in the intracellular distribution of internalized Tf. After 90 min, Tf was still distributed throughout the $a_1$-depleted cells in small vesicular bodies, with partial co-localization with the residual $a_1$ subunit (Fig. 6C, *row 3*, *arrows* and *inset*). A similar distribution pattern was seen after $a_3$ knockdown (Fig. 6C, *row 4*), with some evidence for the presence of larger $a_1$-containing vesicles (*inset* and *arrows*). This was in contrast to the large perinuclear vesicles evident in both control and Ac45-depleted cells, suggesting that subunit $a_{1/3}$ and Ac45 depletion exert their effects at different stages in the endosomal transport process.

## Discussion

In this study, invasive and non-invasive prostate carcinoma cells supported high but essentially indistinguishable overall rates of proton extrusion. The ~36% higher V-ATPase-dependent component of this activity from invasive cells above that from non-invasive was statistically significant, but this difference appears too small to be a critical factor in defining the invasive phenotype. In contrast to previous studies (31, 33), we conclude that in the prostate carcinoma cell lines examined here, V-ATPase function at the plasma membrane differs little between invasive and non-invasive cells. Consequently, we detect no direct correlation between plasma membrane V-ATPase activity and metastatic potential. This does not mean that V-ATPase activity has no role in invasiveness as it clearly does, given that inhibition by either bafilomycin or RNAi has a significant impact on invasiveness (31, 33). Rather than being a feature that distinguishes invasive from non-invasive cells, we suggest that plasma membrane V-ATPase facilitates invasiveness by supporting ECM degradation via extracellular acidification or transport/secretion of protease cargo (32, 65–67). This latter role is consistent with the observation that Ac45 knockdown decreases invasiveness with only a small loss of $J_H^+$, presumably as a consequence of stalling transport processes (discussed below).

The microscopy data and RNAi effects on TfR recycling indicate that the $a_1$ and $a_3$ isoforms primarily operate in different

endosome populations. The distribution of the $a_1$ isoform within the cell strongly resembles that of TfR (Fig. 3), suggesting that it also transits through early endosomes and recycles back to the plasma membrane (68, 69). Bafilomycin brings about rapid alkalinization of compartments along the endosome-lysosome route but has only a small effect on the rate of TfR internalization from the plasma membrane (70) or trafficking of cargo from the sorting endosome to the endosomal recycling compartment (ERC) (71, 72). In contrast, bafilomycin significantly slows exit of cargo from the ERC (72), suggesting that it is this stage in the recycling process that is most affected by loss of V-ATPase activity after RNAi depletion of $a_1$. The $a_3$ form largely populates late endosomes/lysosomes, yet it also traffics to the plasma membrane. This isoform is recruited from late endosomes/lysosomes to plasma membrane-derived structures in macrophages and in osteoclasts via interaction with microfilaments (14, 18, 73). A general role in secretory pathways has been proposed for this isoform (24) that could extend to the prostatic epithelial cells examined here, where it could be present on secretory lysosomes. It is noteworthy that both $a_1$ and $a_3$ knockdown decrease Tf internalization, slowing its transit through the endosome network. Depletion of either $a$ subunit also leads to significant differences in morphology and intracellular distribution of TfR/$a_1$ vesicles compared with control cells (and to Ac45-depleted cells, discussed below) visualized by antibody staining or chase of fluorescent Tf ligand through the transport pathways. Complete and efficient trafficking of the Tf-TfR complex through the endosomal system must therefore require both $a_1$ and $a_3$ forms of the V-ATPase. Given that subunit A knockdown leads to a slowing of TfR recycling similar to that seen with $a_1$ (and to a lesser extent $a_3$), it seems most plausible that this retention effect results from loss of V-ATPase activity. Of course this does not exclude the possibility that loss of $V_o$ resulting from $a_1$ (or $a_3$) knockdown also prevents a final (ATPase-independent) membrane fusion process at the plasma membrane perhaps involving a connection to the R-SNARE.

In the degradative pathway, the movement of cargo from the late endosome to lysosome (but not entry into the late endosome) is also dependent on V-ATPase activity (71, 74). Here, knockdown of either $a_1$ or $a_3$ isoforms (also Ac45) had an effect on this process, inhibiting the overall level of dextran uptake into the cell. However, because this FITC-dextran uptake was inhibited without any apparent alkalinization of the late endosomes/lysosome, we conclude that knockdown of the V-ATPase must lead to overall loss of cellular capacity for fluid-phase endocytosis and transition to the lysosome but with the residual V-ATPase expression still sufficient to achieve normal luminal pH.

Recruitment of proteins to endosomal membranes is pH-dependent (75, 76), and hence V-ATPase proton-pumping capacity is important in defining the function of the compartment. Here, $a_1$ and $a_3$ isoforms were differentially targeted to cellular compartments that have different luminal pH ($>6$ for $a_1$ in early endosomes/ERC and $<6$ for $a_3$ in late endosomes/lysosomes). An intriguing possibility is that the presence of $a_1$ or $a_3$ programs the V-ATPase to maintain a particular luminal pH. This could result from perhaps different ATP/H$^+$ coupling ratios (77) or via a pH-sensing regulatory feedback system with similarities to that proposed for the $a_2$ subunit isoform (78).

The $V_o$-associated glycoprotein Ac45 (ATP6AP1 and ATP6S1) plays a major role in navigating the V-ATPase around prostate carcinoma cells, as it does in the secretory pathway of neuroendocrine cells (49). The question is as follows. Does Ac45 facilitate transport to the plasma membrane, internalization from the plasma membrane, or both stages in the transport process? Ac45 does function in clathrin-coated vesicle formation and clathrin-mediated endocytosis (79), with internalization from the plasma membrane mediated via recognition sequences in its 26-residue cytoplasmic tail (80). Consistent with a function in guiding the V-ATPase to the plasma membrane, mutations in this same cytoplasmic tail lead to failure to recruit $a_3$-containing V-ATPase to the ruffled membrane of osteoclasts (48). Ac45 transgene expression has furthermore been shown to cause V-ATPase accumulation at the plasma membrane (49). Consequently, roles in transport both to and from the plasma membrane are supported, albeit in different cell types. This is reiterated here in invasive prostate carcinoma cells, although Ac45 depletion appears to have a predominant effect on transit to the plasma membrane. The partial loss of plasma membrane V-ATPase activity in Ac45-depleted cells indicates a net decrease in V-ATPase transport to the plasma membrane, although we have been unable to determine whether just $a_1$ or both $a_1$ and $a_3$ isoforms are affected. However, based on their shared contribution to the overall $J_H^+$ in PC-3 cells, both are likely to be affected to some extent. Most significantly, Ac45 knockdown also arrests recycling of Tf and TfR. During chase experiments, the morphology and organization of transferrin-loaded vesicles in Ac45-depleted cells was very similar to that in control cells, suggesting that Tf-TfR was retained at a relatively late stage in the recycling process by failing to exit the ERC or linked to a function of Ac45 in late-stage exocytosis (50). Incomplete knockdown of $a_1$ or $a_3$ had similar effects to Ac45 depletion on recycling of TfR, but the differences in vesicle morphology resulting from these knockdown experiments implies that they affect the process at a different earlier stage. Ac45 depletion also had some effect on the kinetics of internalization of TfR and the $a_1$ isoform, slowing their removal from the plasma membrane, again consistent with the reported effects of V-ATPase subunit depletion on endocytosis (79). We therefore conclude that although Ac45 is an important factor in navigating the V-ATPase through the endosomal system, the effect of its knockdown is not simply due to a failure to bring the acidifying enzyme to the correct compartment. Instead, its role is in targeting the V-ATPase to the correct place in the late stages of membrane fusion during exocytosis. If Ac45 is a significant factor in navigating the V-ATPase to the plasma membrane, enhanced expression could be responsible for maintaining the high levels of surface V-ATPase activity in cancer cells.

## References

1. Sennoune, S. R., Bakunts, K., Martínez, G. M., Chua-Tuan, J. L., Kebir, Y., Attaya, M. N., and Martínez-Zaguilán, R. (2004) Vacuolar H$^+$-ATPase in human breast cancer cells with distinct metastatic potential: distribution and functional activity. *Am. J. Physiol. Cell Physiol.* **286,** C1443–C1452

2. Martinez-Zaguilan, R., Lynch, R. M., Martinez, G. M., and Gillies, R. J. (1993) Vacuolar-type H$^+$-ATPases are functionally expressed in plasma membranes of human tumor cells. *Am. J. Physiol.* **265,** C1015–C1029

3. Cotter, K., Capecci, J., Sennoune, S., Huss, M., Maier, M., Martinez-Zaguilan, R., and Forgac, M. (2015) Activity of plasma membrane V-ATPases is critical for the invasion of MDA-MB231 breast cancer cells. *J. Biol. Chem.* **290,** 3680–3692

4. Sennoune, S. R., and Martinez-Zaguilan, R. (2007) Plasmalemmal vacuolar H$^+$-ATPases in angiogenesis, diabetes and cancer. *J. Bioenerg. Biomembr.* **39,** 427–433

5. Muench, S. P., Trinick, J., and Harrison, M. A. (2011) Structural divergence of the rotary ATPases. *Q. Rev. Biophys.* **44,** 311–356

6. Marshansky, V., Rubinstein, J. L., and Grüber, G. (2014) Eukaryotic V-ATPase: novel structural findings and functional insights. *Biochim. Biophys. Acta* **1837,** 857–879

7. Forgac, M. (2007) Vacuolar ATPases: rotary proton pumps in physiology and pathophysiology. *Nat. Rev. Mol. Cell Biol.* **8,** 917–929

8. Breton, S., and Brown, D. (2013) Regulation of luminal acidification by V-ATPase. *Physiology* **28,** 318–329

9. Toei, M., Saum, R., and Forgac, M. (2010) Regulation and isoform function of the V-ATPases. *Biochemistry* **49,** 4715–4723

10. Sun-Wada, G. H., and Wada, Y. (2010) Vacuolar-type proton pump ATPases: roles of subunit isoforms in physiology and pathology. *Histol. Histopathol.* **25,** 1611–1620

11. Karet, F. E., Finberg, K. E., Nelson, R. D., Nayir, A., Mocan, H., Sanjad, S. A., Rodriguez-Soriano, J., Santos, F., Cremers, C. W., Di Pietro, A., Hoffbrand, B. I., Winiarski, J., Bakkaloglu, A., Ozen, S., Dusunsel, R., *et al.* (1999) Mutations in the gene encoding B1 subunit of H$^+$-ATPase cause renal tubular acidosis with sensorineural deafness. *Nat. Genet.* **21,** 84–90

12. Toyomura, T., Oka, T., Yamaguchi, C., Wada, Y., and Futai, M. (2000) Three subunit a isoforms of mouse vacuolar H$^+$-ATPase. Preferential expression of the a3 isoform during osteoclast differentiation. *J. Biol. Chem.* **275,** 8760–8765

13. Nishi, T., and Forgac, M. (2000) Molecular cloning and expression of three isoforms of the 100-kDa a subunit of the mouse vacuolar proton-translocating ATPase. *J. Biol. Chem.* **275,** 6824–6830

14. Toyomura, T., Murata, Y., Yamamoto, A., Oka, T., Sun-Wada, G. H., Wada, Y., and Futai, M. (2003) From lysosomes to the plasma membrane: localization of vacuolar type H$^+$-ATPase with the a3 isoform during osteoclast differentiation. *J. Biol. Chem.* **278,** 22023–22030

15. Marshansky, V., and Futai, M. (2008) The V-type H$^+$-ATPase in vesicular trafficking: targeting, regulation and function. *Curr. Opin. Cell Biol.* **20,** 415–426

16. Kawasaki-Nishi, S., Bowers, K., Nishi, T., Forgac, M., and Stevens, T. H. (2001) The amino-terminal domain of the vacuolar proton-translocating ATPase a-subunit controls targeting and *in vivo* dissociation, and the carboxyl-terminal domain affects coupling of proton transport and ATP hydrolysis. *J. Biol. Chem.* **276,** 47411–47420

17. Morel, N., Dedieu, J. C., and Philippe, J. M. (2003) Specific sorting of the a1 isoform of the V-H$^+$ATPase a subunit to nerve terminals where it associates with both synaptic vesicles and the presynaptic plasma membrane. *J. Cell Sci.* **116,** 4751–4762

18. Sun-Wada, G. H., Tabata, H., Kawamura, N., Aoyama, M., and Wada, Y. (2009) Direct recruitment of H$^+$-ATPase from lysosomes for phagosomal acidification. *J. Cell Sci.* **122,** 2504–2513

19. Smith, A. N., Skaug, J., Choate, K. A., Nayir, A., Bakkaloglu, A., Ozen, S., Hulton, S. A., Sanjad, S. A., Al-Sabban, E. A., Lifton, R. P., Scherer, S. W., and Karet, F. E. (2000) Mutations in ATP6N1B, encoding a new kidney vacuolar proton pump 116-kD subunit, cause recessive distal renal tubular acidosis with preserved hearing. *Nat. Genet.* **26,** 71–75

20. Oka, T., Murata, Y., Namba, M., Yoshimizu, T., Toyomura, T., Yamamoto, A., Sun-Wada, G. H., Hamasaki, N., Wada, Y., and Futai, M. (2001) α4, a unique kidney-specific isoform of mouse vacuolar H$^+$-ATPase subunit a. *J. Biol. Chem.* **276,** 40050–40054

21. Hurtado-Lorenzo, A., Skinner, M., El Annan, J., Futai, M., Sun-Wada, G. H., Bourgoin, S., Casanova, J., Wildeman, A., Bechoua, S., Ausiello, D. A., Brown, D., and Marshansky, V. (2006) V-ATPase interacts with ARNO and Arf6 in early endosomes and regulates the protein degradative pathway. *Nat. Cell Biol.* **8,** 124–136

22. Kornak, U., Reynders, E., Dimopoulou, A., van Reeuwijk, J., Fischer, B., Rajab, A., Budde, B., Nürnberg, P., Foulquier, F., ARCL Debré-type Study Group, Lefeber, D., Urban, Z., Gruenewald, S., Annaert, W., Brunner, H. G., *et al.* (2008) Impaired glycosylation and cutis laxa caused by mutations in the vesicular H$^+$-ATPase subunit ATP6V0A2. *Nat. Genet.* **40,** 32–34

23. Saw, N. M., Kang, S. Y., Parsaud, L., Han, G. A., Jiang, T., Grzegorczyk, K., Surkont, M., Sun-Wada, G. H., Wada, Y., Li, L., and Sugita, S. (2011) Vacuolar H$^+$-ATPase subunits Voa1 and Voa2 cooperatively regulate secretory vesicle acidification, transmitter uptake, and storage. *Mol. Biol. Cell* **22,** 3394–3409

24. Sun-Wada, G. H., Toyomura, T., Murata, Y., Yamamoto, A., Futai, M., and Wada, Y. (2006) The a3 isoform of V-ATPase regulates insulin secretion from pancreatic beta-cells. *J. Cell Sci.* **119,** 4531–4540

25. Wang, D., Epstein, D., Khalaf, O., Srinivasan, S., Williamson, W. R., Fayyazuddin, A., Quiocho, F. A., and Hiesinger, P. R. (2014) Ca$^{2+}$ calmodulin regulates SNARE assembly and spontaneous neurotransmitter release via v-ATPase subunit V0a1. *J. Cell Biol.* **205,** 21–31

26. Di Giovanni, J., Boudkkazi, S., Mochida, S., Bialowas, A., Samari, N., Lévêque, C., Youssouf, F., Brechet, A., Iborra, C., Maulet, Y., Moutot, N., Debanne, D., Seagar, M., and El Far, O. (2010) V-ATPase membrane sector associates with synaptobrevin to modulate neurotransmitter release. *Neuron* **67,** 268–279

27. Pietrement, C., Sun-Wada, G. H., Silva, N. D., McKee, M., Marshansky, V., Brown, D., Futai, M., and Breton, S. (2006) Distinct expression patterns of different subunit isoforms of the V-ATPase in the rat epididymis. *Biol. Reprod.* **74,** 185–194

28. Montcourrier, P., Silver, I., Farnoud, R., Bird, I., and Rochefort, H. (1997) Breast cancer cells have a high capacity to acidify extracellular milieu by a dual mechanism. *Clin. Exp. Metastasis* **15,** 382–392

29. Martínez-Zaguilán, R., Raghunand, N., Lynch, R. M., Bellamy, W., Martinez, G. M., Rojas, B., Smith, D., Dalton, W. S., and Gillies, R. J. (1999) pH and drug resistance. I. Functional expression of plasmalemmal V-type H$^+$-ATPase in drug-resistant human breast carcinoma cell lines. *Biochem. Pharmacol.* **57,** 1037–1046

30. Xu, X., You, J., and Pei, F. (2012) Silencing of a novel tumor metastasis suppressor gene LASS2/TMSG1 promotes invasion of prostate cancer cell *in vitro* through increase of vacuolar ATPase activity. *J. Cell. Biochem.* **113,** 2356–2363

31. Michel, V., Licon-Munoz, Y., Trujillo, K., Bisoffi, M., and Parra, K. J. (2013) Inhibitors of vacuolar ATPase proton pumps inhibit human prostate cancer cell invasion and prostate-specific antigen expression and secretion. *Int. J. Cancer* **132,** E1–E10

32. Nishisho, T., Hata, K., Nakanishi, M., Morita, Y., Sun-Wada, G. H., Wada, Y., Yasui, N., and Yoneda, T. (2011) The a3 isoform vacuolar type H$^+$-ATPase promotes distant metastasis in the mouse B16 melanoma cells. *Mol. Cancer Res.* **9,** 845–855

33. Hinton, A., Sennoune, S. R., Bond, S., Fang, M., Reuveni, M., Sahagian, G. G., Jay, D., Martinez-Zaguilan, R., and Forgac, M. (2009) Function of a subunit isoforms of the V-ATPase in pH homeostasis and *in vitro* invasion of MDA-MB231 human breast cancer cells. *J. Biol. Chem.* **284,** 16400–16408

34. Gleize, V., Boisselier, B., Marie, Y., Poëa-Guyon, S., Sanson, M., and Morel, N. (2012) The renal v-ATPase a4 subunit is expressed in specific subtypes of human gliomas. *Glia* **60,** 1004–1012

35. Chung, C., Mader, C., Protiva, P., Schmitz, J., Koleske, A., Crawford, S.,

and Gorelick, F. (2010) The vacuolar-ATPase (v-ATPase) confers invasive properties to human pancreatic cancer by modulating MMPs. *Pancreas* **39,** 1315

36. Rozhin, J., Sameni, M., Ziegler, G., and Sloane, B. F. (1994) Pericellular pH affects distribution and secretion of cathepsin-B in malignant cells. *Cancer Res.* **54,** 6517–6525

37. Gillies, R. J., Martinez-Zaguilan, R., Martinez, G. M., Serrano, R., and Perona, R. (1990) Tumorigenic 3T3 cells maintain an alkaline intracellular pH under physiological conditions. *Proc. Natl. Acad. Sci. U.S.A.* **87,** 7414–7418

38. Ishisaki, A., Hashimoto, S., Amagasa, T., and Nishihara, T. (1999) Caspase-3 activation during the process of apoptosis induced by a vacuolar type H$^+$-ATPase inhibitor. *Biol. Cell* **91,** 507–513

39. Sasazawa, Y., Futamura, Y., Tashiro, E., and Imoto, M. (2009) Vacuolar H$^+$-ATPase inhibitors overcome Bcl-xL-mediated chemoresistance through restoration of a caspase-independent apoptotic pathway. *Cancer Sci.* **100,** 1460–1467

40. Luciani, F., Spada, M., De Milito, A., Molinari, A., Rivoltini, L., Montinaro, A., Marra, M., Lugini, L., Logozzi, M., Lozupone, F., Federici, C., Iessi, E., Parmiani, G., Arancia, G., Belardelli, F., and Fais, S. (2004) Effect of proton pump inhibitor pretreatment on resistance of solid tumors to cytotoxic drugs. *J. Natl. Cancer Inst.* **96,** 1702–1713

41. You, H., Jin, J., Shu, H., Yu, B., De Milito, A., Lozupone, F., Deng, Y., Tang, N., Yao, G., Fais, S., Gu, J., and Qin, W. (2009) Small interfering RNA targeting the subunit ATP6L of proton pump V-ATPase overcomes chemoresistance of breast cancer cells. *Cancer Lett.* **280,** 110–119

42. Hernandez, A., Serrano-Bueno, G., Perez-Castineira, J. R., and Serrano, A. (2012) Intracellular proton pumps as targets in chemotherapy: V-ATPases and cancer. *Curr. Pharm. Des.* **18,** 1383–1394

43. De Milito, A., Marino, M. L., and Fais, S. (2012) A rationale for the use of proton pump inhibitors as antineoplastic agents. *Curr. Pharm. Des.* **18,** 1395–1406

44. Huss, M., Ingenhorst, G., König, S., Gassel, M., Dröse, S., Zeeck, A., Altendorf, K., and Wieczorek, H. (2002) Concanamycin A, the specific inhibitor of V-ATPases, binds to the V$_0$ subunit c. *J. Biol. Chem.* **277,** 40544–40548

45. Bowman, E. J., Graham, L. A., Stevens, T. H., and Bowman, B. J. (2004) The bafilomycin/concanamycin binding site in subunit c of the V-ATPases from *Neurospora crassa* and *Saccharomyces cerevisiae. J. Biol. Chem.* **279,** 33131–33138

46. Niikura, K., Takano, M., and Sawada, M. (2004) A novel inhibitor of vacuolar ATPase, FR167356, which can discriminate between osteoclast vacuolar ATPase and lysosomal vacuolar ATPase. *Br. J. Pharmacol.* **142,** 558–566

47. Wang, Y., Inoue, T., and Forgac, M. (2005) Subunit a of the yeast V-ATPase participates in binding of bafilomycin. *J. Biol. Chem.* **280,** 40481–40488

48. Feng, H., Cheng, T., Pavlos, N. J., Yip, K. H., Carrello, A., Seeber, R., Eidne, K., Zheng, M. H., and Xu, J. (2008) Cytoplasmic terminus of vacuolar type proton pump accessory subunit Ac45 is required for proper interaction with V$_0$ domain subunits and efficient osteoclastic bone resorption. *J. Biol. Chem.* **283,** 13194–13204

49. Jansen, E. J., Scheenen, W. J., Hafmans, T. G., and Martens, G. J. (2008) Accessory subunit Ac45 controls the V-ATPase in the regulated secretory pathway. *Biochim. Biophys. Acta* **1783,** 2301–2310

50. Jansen, E. J., van Bakel, N. H., Olde Loohuis, N. F., Hafmans, T. G., Arentsen, T., Coenen, A. J., Scheenen, W. J., and Martens, G. J. (2012) Identification of domains within the V-ATPase accessory subunit Ac45 Involved in V-ATPase transport and Ca$^{2+}$-dependent exocytosis. *J. Biol. Chem.* **287,** 27537–27546

51. Towler, M. C., Prescott, A. R., James, J., Lucocq, J. M., and Ponnambalam, S. (2000) The manganese cation disrupts membrane dynamics along the secretory pathway. *Exp. Cell Res.* **259,** 167–179

52. Dröse, S., Bindseil, K. U., Bowman, E. J., Siebers, A., Zeeck, A., and Altendorf, K. (1993) Inhibitory effects of modified bafilomycins and concanamycins on P- and V-type adenosinetriphosphatases. *Biochemistry* **32,** 3902–3906

53. Nyman, J. K., and Väänänen, H. K. (2010) A rationale for osteoclast selectivity of inhibiting the lysosomal V-ATPase a3 isoform. *Calcif. Tissue Int.* **87,** 273–283

54. Paunescu, T. G., Russo, L. M., Da Silva, N., Kovacikova, J., Mohebbi, N., Van Hoek, A. N., McKee, M., Wagner, C. A., Breton, S., and Brown, D. (2007) Compensatory membrane expression of the V-ATPase B2 subunit isoform in renal medullary intercalated cells of B1-deficient mice. *Am. J. Physiol. Renal Physiol.* **293,** F1915–F1926

55. Manolson, M. F., Wu, B., Proteau, D., Taillon, B. E., Roberts, B. T., Hoyt, M. A., and Jones, E. W. (1994) STV1 gene encodes functional homologue of 95-kDa yeast vacuolar H$^+$-ATPase subunit Vph1p. *J. Biol. Chem.* **269,** 14064–14074

56. Jones, D. H., Nakashima, T., Sanchez, O. H., Kozieradzki, I, Komarova, S. V., Sarosi, I., Morony, S., Rubin, E., Sarao, R., Hojilla, C. V., Komnenovic, V., Kong, Y. Y., Schreiber, M., Dixon, S. J., Sims, S. M., *et al.* (2006) Regulation of cancer cell migration and bone metastasis by RANKL. *Nature* **440,** 692–696

57. Sabbota, A. L., Kim, H. R., Zhe, X., Fridman, R., Bonfil, R. D., and Cher, M. L. (2010) Shedding of RANKL by tumor-associated MT1-MMP activates Src-dependent prostate cancer cell migration. *Cancer Res.* **70,** 5558–5566

58. Peters, C., Bayer, M. J., Bühler, S., Andersen, J. S., Mann, M., and Mayer, A. (2001) Trans-complex formation by proteolipid channels in the terminal phase of membrane fusion. *Nature* **409,** 581–588

59. Hiesinger, P. R., Fayyazuddin, A., Mehta, S. Q., Rosenmund, T., Schulze, K. L., Zhai, R. G., Verstreken, P., Cao, Y., Zhou, Y., Kunz, J., and Bellen, H. J. (2005) The v-ATPase V-0 subunit a1 is required for a late step in synaptic vesicle exocytosis in *Drosophila. Cell* **121,** 607–620

60. Sato, H., Takino, T., Okada, Y., Cao, J., Shinagawa, A., Yamamoto, E., and Seiki, M. (1994) A matrix metalloproteinase expressed on the surface of invasive tumor cells. *Nature* **370,** 61–65

61. Knäuper, V., Will, H., López-Otin, C., Smith, B., Atkinson, S. J., Stanton, H., Hembry, R. M., and Murphy, G. (1996) Cellular mechanisms for human procollagenase-3 (MMP-13) activation– evidence that MT1-MMP (MMP-14) and gelatinase A (MMP-2) are able to generate active enzyme. *J. Biol. Chem.* **271,** 17124–17131

62. Sabeh, F., Li, X. Y., Saunders, T. L., Rowe, R. G., and Weiss, S. J. (2009) Secreted *versus* membrane-anchored collagenases. Relative roles in fibroblast-dependent collagenolysis and invasion. *J. Biol. Chem.* **284,** 23001–23011

63. Macia, E., Ehrlich, M., Massol, R., Boucrot, E., Brunner, C., and Kirchhausen, T. (2006) Dynasore, a cell-permeable inhibitor of dynamin. *Dev. Cell* **10,** 839–850

64. Sheff, D. R., Daro, E. A., Hull, M., and Mellman, I. (1999) The receptor recycling pathway contains two distinct populations of early endosomes with different sorting functions. *J. Cell Biol.* **145,** 123–139

65. Chung, C., Mader, C. C., Schmitz, J. C., Atladottir, J., Fitchev, P., Cornwell, M. L., Koleske, A. J., Crawford, S. E., and Gorelick, F. (2011) The vacuolar-ATPase modulates matrix metalloproteinase isoforms in human pancreatic cancer. *Lab. Investig.* **91,** 732–743

66. Rofstad, E. K., Mathiesen, B., Kindem, K., and Galappathi, K. (2006) Acidic extracellular pH promotes experimental metastasis of human melanoma cells in athymic nude mice. *Cancer Res.* **66,** 6699–6707

67. Lu, X., Qin, W., Li, J., Tan, N., Pan, D., Zhang, H., Xie, L., Yao, G., Shu, H., Yao, M., Wan, D., Gu, J., and Yang, S. (2005) The growth and metastasis of human hepatocellular carcinoma xenografts are inhibited by small interfering RNA targeting to the subunit ATP6L of proton pump. *Cancer Res.* **65,** 6843–6849

68. Mayor, S., Presley, J. F., and Maxfield, F. R. (1993) Sorting of membrane-components from endosomes and subsequent recycling to the cell-surface occurs by a bulk flow process. *J. Cell Biol.* **121,** 1257–1269

69. Maxfield, F. R., and McGraw, T. E. (2004) Endocytic recycling. *Nat. Rev. Mol. Cell Biol.* **5,** 121–132

70. Johnson, L. S., Dunn, K. W., Pytowski, B., and McGraw, T. E. (1993) Endosome acidification and receptor trafficking: bafilomycin A1 slows receptor externalization by a mechanism involving the receptor's internalization motif. *Mol. Biol. Cell* **4,** 1251–1266

71. van Weert, A. W., Dunn, K. W., Geuze, H. J., Maxfield, F. R., and Stoorvogel, W. (1995) Transport from late endosomes to lysosomes, but not sorting of integral membrane-proteins in endosomes, depends on the vac-

uolar proton pump. *J. Cell Biol.* **130,** 821–834

72. Presley, J. F., Mayor, S., McGraw, T. E., Dunn, K. W., and Maxfield, F. R. (1997) Bafilomycin A(1) treatment retards transferrin receptor recycling more than bulk membrane recycling. *J. Biol. Chem.* **272,** 13929–13936

73. Lee, B. S., Gluck, S. L., and Holliday, L. S. (1999) Interaction between vacuolar H$^+$-ATPase and microfilaments during osteoclast activation. *J. Biol. Chem.* **274,** 29164–29171

74. Baravalle, G., Schober, D., Huber, M., Bayer, N., Murphy, R. F., and Fuchs, R. (2005) Transferrin recycling and dextran transport to lysosomes is differentially affected by bafilomycin, nocodazole, and low temperature. *Cell Tissue Res.* **320,** 99–113

75. Aniento, F., Gu, F., Parton, R. G., and Gruenberg, J. (1996) An endosomal $\beta$-COP is involved in the pH-dependent formation of transport vesicles destined for late endosomes. *J. Cell Biol.* **133,** 29–41

76. Clague, M. J., Urbé, S., Aniento, F., and Gruenberg, J. (1994) V-ATPase activity is required for endosomal carrier vesicle formation. *J. Biol. Chem.* **269,** 21–24

77. Kawasaki-Nishi, S., Nishi, T., and Forgac, M. (2001) Yeast V-ATPase complexes containing different isoforms of the 100-kDa a-subunit differ in coupling efficiency and *in vivo* dissociation. *J. Biol. Chem.* **276,** 17941–17948

78. Marshansky, V. (2007) The V-ATPase a2-subunit as a putative endosomal pH sensor. *Biochem. Soc. Trans.* **35,** 1092–1099

79. Kozik, P., Hodson, N. A., Sahlender, D. A., Simecek, N., Soromani, C., Wu, J., Collinson, L. M., and Robinson, M. S. (2013) A human genome-wide screen for regulators of clathrin-coated vesicle formation reveals an unexpected role for the V-ATPase. *Nat. Cell Biol.* **15,** 50–60

80. Jansen, E. J., Holthuis, J. C., McGrouther, C., Burbach, J. P., and Martens, G. J. (1998) Intracellular trafficking of the vacuolar H$^+$-ATPase accessory subunit Ac45. *J. Cell Sci.* **111,** 2999–3006

**Extracellular and Luminal pH Regulation by Vacuolar H⁺-ATPase Isoform**
$$\text{Extracellular and Luminal pH Regulation by Vacuolar H}^{+}\text{-ATPase Isoform}$$

# Extracellular and Luminal pH Regulation by Vacuolar H$^{+}$-ATPase Isoform Expression and Targeting to the Plasma Membrane and Endosomes

Gina A. Smith, Gareth J. Howell, Clair Phillips, Stephen P. Muench, Sreenivasan Ponnambalam and Michael A. Harrison

Access the most updated version of this article at doi: 10.1074/jbc.M116.723395

Alerts:
- When this article is cited
- When a correction for this article is posted

Click here to choose from all of JBC's e-mail alerts

This article cites 80 references, 42 of which can be accessed free at
http://www.jbc.org/content/291/16/8500.full.html#ref-list-1